TKK Dissertations 112
Espoo 2008

MICROELECTROMECHANICAL RESONATORS FOR FREQUENCY REFERENCE AND FREQUENCY CONVERSION APPLICATIONS

Doctoral Dissertation

Mika Koskenvuori

Helsinki University of Technology
Faculty of Electronics, Communications and Automation
Department of Micro and Nanosciences

TKK Dissertations 112
Espoo 2008

MICROELECTROMECHANICAL RESONATORS FOR FREQUENCY REFERENCE AND FREQUENCY CONVERSION APPLICATIONS

Doctoral Dissertation

Mika Koskenvuori

Dissertation for the degree of Doctor of Science in Technology to be presented with due permission of the Faculty of Electronics, Communications and Automation for public examination and debate in Large Seminar Hall of Micronova at Helsinki University of Technology (Espoo, Finland) on the 4th of April, 2008, at 12 noon.

Helsinki University of Technology
Faculty of Electronics, Communications and Automation
Department of Micro and Nanosciences

Teknillinen korkeakoulu
Elektroniikan, tietoliikenteen ja automaation tiedekunta
Mikro- ja nanotekniikan laitos

Distribution:
Helsinki University of Technology
Faculty of Electronics, Communications and Automation
Department of Micro and Nanosciences
P.O. Box 3500
FI - 02015 TKK
FINLAND
URL: http://www.micronova.fi/units/mns
Tel. +358-9-4511
Fax +358-9-451 3128
E-mail: mika.koskenvuori@tkk.fi

ISBN 978-951-22-9278-3
ISBN 978-951-22-9279-0 (PDF)
ISSN 1795-2239
ISSN 1795-4584 (PDF)
URL: http://lib.tkk.fi/Diss/2008/isbn9789512292790/

TKK-DISS-2449

Multiprint Oy
Espoo 2008

ABSTRACT OF DOCTORAL DISSERTATION	HELSINKI UNIVERSITY OF TECHNOLOGY P.O. BOX 1000, FI-02015 TKK http://www.tkk.fi

Author Mika Petteri Koskenvuori

Name of the dissertation
Microelectromechanical resonators for frequency reference and frequency conversion applications

Manuscript submitted 07.12.2007	Manuscript revised 03.03.2008
Date of the defence 04.04.2008	
☐ Monograph	☒ Article dissertation (summary + original articles)

Faculty Faculty of Electronics, Communications and Automation
Department Department of Micro and Nanosciences
Field of research Microsystems
Opponent(s) prof. Gabriel Abadal
Supervisor prof. Ilkka Tittonen

Abstract

Microelectromechanical systems (MEMS) have been used in sensor applications for more than three decades. With improvements in design and microfabrication, MEMS based solutions are also entering the field of RF electronics.

In this thesis, the main emphasis is laid on two different capacitively coupled resonant micromechanical systems, which are the frequency reference and frequency down-converter. It is shown that a high precision frequency reference with the stability comparable to a macroscopic quartz oscillator can be realised using a micromechanical silicon resonator. An oscillator with a phase-noise of $\mathscr{L}_f$ = -138 dBc/Hz at Δf = 1 kHz offset from the f_c = 13 MHz carrier and with a noise-floor of $\mathscr{L}$ = -150 dBc/Hz is realised with a bulk acoustic vibrational mode. It is also shown that the long-term stability of the encapsulated resonators is sufficient for high precision frequency references: the measured frequency stability is $\Delta f/f < \pm 1$ ppm for a period of t = 1000 h with a drift of $|\Delta f/\Delta t| < (1.15 - 5.25)\times 10^{-4}$ Hz/h. These results suggest that the demands on the centre frequency stability, which is usually specified for a time scale of one year for various frequency references in wireless communication, can be fulfilled. For a more detailed study of the instability mechanisms of capacitive MEMS devices a fast method to measure the built-in potentials is presented. Two approaches to convert the high frequency input signal down to the mechanical resonance frequency of the MEMS-devices using micromechanical mixers are demonstrated. In the first method a local oscillator signal is used to perform the conversion to the carrier signal at f_c = 390 MHz. The second method leads to an intrinsic conversion of an AM-modulated signal without any local oscillator. This conversion is demonstrated up to f_c = 1.5 GHz. The second method is used to perform the demodulation of a signal carrying a few bits of information in a micromechanical radio.

Parametric amplification is suggested as a low-noise method to improve the conversion performance of micromechanical mixers. An improvement of the conversion performance by more than 30 dB is demonstrated. Novel approaches to improve the conversion are suggested through mathematical simulations.

A fabrication process combining atomic layer deposition, electron beam lithography and cryogenic etching is demonstrated. The process can be used for fast prototyping of MEMS-devices at least for research purposes. As a result a few micromechanical resonators can be fabricated in a few hours time from the original design without the need of using a metallic photomask but applying a direct electron beam writing in lithography.

Keywords Micromechanics, resonator, stability, reference oscillator, frequency conversion, fabrication

ISBN (printed) 978-951-22-9278-3	ISSN (printed) 1795-2239
ISBN (pdf) 978-951-22-9279-0	ISSN (pdf) 1795-4584
Language English	Number of pages 61 + 48

Publisher Helsinki University of Technology, Department of Micro and Nanosciences

Print distribution Helsinki University of Technology, Department of Micro and Nanosciences

☒ The dissertation can be read at http://lib.tkk.fi/Diss/2008/isbn9789512292790/

VÄITÖSKIRJAN TIIVISTELMÄ	TEKNILLINEN KORKEAKOULU PL 1000, 02015 TKK http://www.tkk.fi

Tekijä Mika Petteri Koskenvuori

Väitöskirjan nimi
Mikroeletromekaaniset resonaattorit taajuusreferenssi- ja taajuusmuunnossovelluksissa

Käsikirjoituksen päivämäärä 07.12.2007	Korjatun käsikirjoituksen päivämäärä 03.03.2008

Väitöstilaisuuden ajankohta 04.04.2008

☐ Monografia	☒ Yhdistelmäväitöskirja (yhteenveto + erillisartikkelit)

Tiedekunta Elektroniikan, tietoliikenteen ja automaation tiedekunta
Laitos Mikro- ja nanotekniikan laitos
Tutkimusala Mikrosysteemit
Vastaväittäjä(t) prof. Gabriel Abadal
Työn valvoja prof. Ilkka Tittonen

Tiivistelmä

Mikroelektromekaania systeemejä (MEMS) on käytetty anturisovelluksissa jo yli kolmenkymmenen vuoden ajan. Parantuneiden suunnittelu- ja laskentamenetelmien sekä valmistustekniikan kehityksen ansiosta MEMS-pohjaisia ratkaisuja käytetään myös radiotaajuisissa elektroniikkapiireissä.

Tässä työssä tutkitaan kahta mikrosysteemiä, jotka voidaan toteuttaa kapasitiivisesti kytketyn mikromekaanisen värähtelijän avulla: taajuusreferenssi ja signaalin alassekoitin. Työssä osoitetaan, että piistä valmistettua mikromekaanista värähtelijää käyttämällä on mahdollista valmistaa hyvin tarkka taajuusreferenssi, jonka stabiilisuus on jopa kvartsikiteestä valmistetun oskillaattorin luokkaa. Osoituksena tästä oskillaattori, jonka vaihekohina on $\mathscr{L}_f$ = -138 dBc/Hz Δf = 1 kHz päässä kantoaallosta pohjakohinan ollessa $\mathscr{L}$ = -150 dBc/Hz toteutetaan piivärähtelijää käyttämällä. Työssä osoitetaan myös, että pakattujen värähtelijöiden pitkän ajan stabiilisuus on riittävä suuren tarkkuuden taajuusreferenssisovelluksissa. Mitatuksi taajuuspoikkeamaksi saatiin $\Delta f/f < \pm 1$ ppm t = 1000 h mittausjaksolla, taajuusryöminnän ollessa $|\Delta f/\Delta t| < (1.15 - 5.25)\times10^{-4}$ Hz/h. Näiden tulosten perusteella värähtelijöiden pitkän ajan stabiilisuus näyttää riittävältä langattomassa tiedonsiirrossa käytettävien taajuusreferenssien toteuttamiseen. Kapasitiivisten rakenteiden epävarmuustekijöiden tarkempaan analysointiin esitetään menetelmä ns. built-in jännitteen mittaamiseksi.

Työssä tutkitaan kahta menetelmää korkeataajuisen signaalin muuntamiseksi mikromekaanisten värähtelijöiden mekaaniselle resonanssitaajuudelle. Muunnos tehdään käyttämällä mikromekaanista värähtelijää taajuussekoittimena. Ensimmäisessä menetelmässä muunnos suoritetaan paikallisoskillaattorin avulla f_c = 390 MHz:n kantoaallolle. Toinen menetelmä perustuu AM-moduloidun signaalin itsenäiseen muunnokseen ilman paikallisoskillaattoria. Tämän menetelmän toimivuus osoitetaan jopa f_c = 1.5 GHz:n kantoaallolle. Toisen menetelmän avulla demonstroidaan miten muutaman bitin verran informaatiota saadaan luettua radiotaajuisesta signaalista ns. mikromekaanisen radion avulla.

Parametrista vahvistusta ehdotetaan ratkaisuksi mikromekaanisen sekoittimen muuntosuhteen parantamiseksi. Työssä mitataan yli 30 dB:n parannus käyttämällä parametrista vahvistusta. Lisäksi ehdotetaan muita ratkaisuja muuntosuhteen parantamiseksi – nämä ratkaisut todennetaan matemaattisilla simulaatioilla.

Lisäksi kuvataan valmistusprosessi, joka mahdollistaa MEMS-rakenteiden nopean valmistuksen ainakin tutkimuskäyttöön. Prosessi yhdistää atomikerroskasvatuksen, elektronisuihku-litografian sekä kryogeenisen kuivasyövytyksen ja sen avulla voidaan tuottaa pieniä määriä laadukkaita MEMS-rakenteita muutamassa tunnissa. Menetelmässä rakenne valotetaan suoraan piisirun pinnalle elektronisuihkulitografialla, joten erillistä metallista valotusmaskia ei tarvita.

Asiasanat Mikromekaniikka, värähtelijä, stabiilisuus, referenssioskillaattori, taajuus sekoitus, valmistus

ISBN (painettu) 978-951-22-9278-3	ISSN (painettu) 1795-2239
ISBN (pdf) 978-951-22-9279-0	ISSN (pdf) 1795-4584
Kieli englanti	Sivumäärä 61 + 48

Julkaisija Teknillinen korkeakoulu, Mikro- ja nanotekniikan laitos

Painetun väitöskirjan jakelu Teknillinen korkeakoulu, Mikro- ja nanotekniikan laitos

☒ Luettavissa verkossa osoitteessa http://lib.tkk.fi/Diss/2008/isbn9789512292790/

Contents

Acknowledgement

The work leading to this thesis has been carried out during the years 2002-2007 and has been supported by many people. I probably can not remember everyone, but do not be offended if you are not on the list.

First I would like to thank prof. Ilkka Tittonen for giving me the opportunity to work in the research group and for the guidance and supervision at all the stages of the work that has led to this thesis.

Secondly I would like to thank all my colleagues and co-workers in the Metrology Research Institute, Optics and molecular materials and Micro and nanosciences laboratory. Most of all, I would like to thank all the co-authors of the publications. Especially I would like to mention Pekka Rantakari with whom a great deal of work that did not ever make into the journals was done, but at least in the end one journal article was published with the names of us both. I would also like to thank my office-mates: Nikolai Chekurov, Päivi Sievilä and Ossi Hahtela for the discussions related to work and leisure.

Of the people outside the laboratory I would like to thank Dr. Tomi Mattila especially for the help with my first first-authored journal publication, which gave me a great deal of self-confidence to continue the pursuit of the doctoral degree. Dr. Ari Alastalo deserves my gratitude for fruitful discussions and collaboration especially during the second part of the work. My gratitude goes also to my other superior Dr. Runar Törnqvist for giving me the opportunity to work with the UMK - Center for New Materials and for the faith in my abilities. Working at the UMK has really been a needed alternative for the research work in the laboratory. For other balancing acts between work and life I would like to thank all my friends - You know who you are.

For financially supporting this thesis work I would like to gratefully acknowledge Jenny and Antti Wihuri Foundation and Finnish Academy of Science and Letters – Vilho, Yrjö and Kalle Väisälä Foundation.

I would like to express my warm thanks to my mother for giving me the background from which to continue this far. My kids: Jari, Tiia and Anselmi deserve thanks for keeping me inspired in the process that has led to this thesis – Every doctoral student should be envious about the speed that kids learn new stuff.

Finally, I owe my deepest gratitude for my loving wife, Suvi, for all the support she has given me and for being the one to believe that I will accomplish this task even during the times I have not believed it myself.

Espoo, Independence Day of 2007

Mika Koskenvuori

List of publications

This dissertation consists of an overview and the following papers published in international refereed journals:

[P1] T. Mattila, V. Kaajakari, J. Kiihamäki, A. Oja, H. Kattelus, H. Seppä, M. Koskenvuori, P. Rantakari, and I. Tittonen, "Silicon Micromechanical Resonators for RF-Applications", *Physica Scripta*, **T114**, pp. 181-183 (2004)

[P2] M. Koskenvuori, T. Mattila, A. Häärä, J Kiihamäki, A. Oja, H. Seppä and I. Tittonen, "Long-term stability of single-crystal silicon microresonators", *Sensors and Actuators A: Physical*, **115,** pp. 23-27 (2004)

[P3] M. Koskenvuori and I. Tittonen, "GHz-range FSK-reception with microelectromechanical resonators", Accepted for publication in *Sensors and Actuators A: Physical,* **142**, pp. 346-351 (2008)

[P4] N. Chekurov, M. Koskenvuori, V-M. Airaksinen, and I. Tittonen, "Atomic layer deposition enhanced rapid dry fabrication of micromechanical devices with cryogenic deep reactive ion etching", *Journal of Micromechanics and Microengineering*, **17**, pp. 1731-1736 (2007)

[P5] M. Koskenvuori, V-P. Rytkönen, P. Rantakari and I. Tittonen, "Kelvin-probe type method for the fast measurement of built-in voltage inside closed cavity MEMS-devices", *Journal of Physics D: Applied Physics,* **40**, pp. 5558-5563 (2007)

[P6] M. Koskenvuori and I. Tittonen, "Parametric amplification of a resonating multimode micromechanical mixer-filter", *IEEE Electron Device Letters*, **28**, pp. 970-972 (2007)

[P7] M. Koskenvuori and I. Tittonen, "Towards micromechanical radio: overtone excitations of a microresonator through the nonlinearities of the 2^{nd} and 3^{rd} order", Accepted for publication in *IEEE Journal of Microelectromechanical Systems*

Author's contribution

For publication P1 the author performed the long-term stability measurements and participated in the design and characterization of the resonator used for short-term stability measurements.

For publication P2 the author prepared the manuscript and performed all the measurements.

For publication P3 the author prepared the manuscript and performed all the measurements and simulations.

For publication P4 the author prepared the manuscript and designed the initial fabrication process. The author also participated in the optimization and characterization of the process and designed the test-components and actual devices fabricated with the method. The author also performed all the measurements, simulations and calculations concerning the fabricated devices.

For publication P5 the author prepared the manuscript and planned and supervised the measurements and the construction of the measurement set-up.

For publication P6 the author prepared the manuscript and performed all the measurements and simulations.

For publication P7 the author prepared the manuscript and performed all the measurements and simulations.

In addition, the author has presented the results of the work at international conferences such as IEEE MEMS (2008), Transducers (2007), ICMAT (2007), Eurosensors (2002-2004, 2006), IEEE Ultrasonics Symposium (2002) and MFMN (2002).

Symbols

A	Area of a transducer ($A = L_e \times h$)
c	Concentration
C	Capacitance
C_m	Mechanical equivalent capacitance
C_{pad}	Capacitance of a bonding pad
C_0	Capacitance of a transducer at rest ($C_0 = A \times \varepsilon_0/d$)
d	(Coupling) gap width
E	Energy of a capacitor
E_{vib}	Mechanical vibration energy
f_c	Carrier frequency
f_m	Modulation frequency
f_{res}	Resonance frequency
F	(Periodic) Force
G	Gain
h	Height of a device
m	Mass
k	Spring constant
k_0	Unmodulated spring constant
k_b	Boltzmann constant ($=1.38\times10^{-23}$ kg·m^2/(K·s^2))
$k_{e(n)}$	Electrical spring constant (of the order n)
k_m	Mechanical spring constant
L	Length of a device
L_e	Length of a transducer
L_m	Mechanical equivalent inductance
p	Pressure
P_c	Power consumption
Q	(Mechanical) Quality factor or charge
R_m	Mechanical equivalent resistance
t	Time
T	Temperature
u	(ac) voltage
u_n	Noise voltage
U	(DC) Voltage
U_{DC}	DC bias-voltage
U_{pi}	Pull-in voltage
V_{bi}	Built-in potential
w	Width of a device or width of a transducer
x	Displacement or vibration amplitude
x_c	Critical vibration amplitude
α	Capacitance ratio
β	Relative amplitude of vibration ($\beta = x/d$)
ε	Permittivity
ε_0	Permittivity of vacuum ($=1.38\times10^{-12}$ F/m)
γ	Damping constant
η	Electromechanical coupling constant or transduction factor
κ	Frequency shift due to the non-linearities

λ	Wavelength
ψ	Bias-voltage sensitivity factor of the frequency
τ	Time-constant
φ	Phase difference
ω	Angular frequency
$\mathscr{L}_f$	Phase noise at certain offset from the carrier frequency
$\mathscr{L}$	Noise floor

Abbreviations

ALD	Atomic layer deposition
AM	Amplitude modulation
BAW	Bulk-acoustic-wave
CL	Conversion loss
C-V	Capacitance-voltage
DETF	Double-ended-tuning-fork
DRIE	Deep reactive ion etching
E-beam	Electron beam
FBAR	Film bulk acoustic resonator
FSK	Frequency-shift-keying
GSM	Global system for mobile communications
HB	Harmonic balance
HF	Hydrofluoric (acid)
IC	Integrated circuit
IF	Intermediate frequency
IM(3)	(Third order) Intermodulation distortion
LO	Local oscillator
MEMS	Microelectromechanicalsystem
OCXO	Oven Controlled Crystal (X-tal) Oscillator
OFDM	Orthogonal Frequency Division Multiplexing
OOK	On-off-keying
PLL	Phase-locked loop
PMMA	Polymethylmetacrylate
RF	Radio frequency
RH	Relative humidity
RIE	Reactive ion etching
SAM	Self-assembled/assemblying monolayer
SE-BAW	Square-extensional Bulk-acoustic-wave
SEM	Scanning electron microscope
SOI	Silicon-on-insulator
VCO	Voltage-controlled oscillator

1 Introduction

Micromechanical or microfabricated devices have been used in commercialised pressure sensors transducers for more than three decades [1]. The recent advances in the fabrication methods of microelectromechanical systems (MEMS) have opened the possibility of using microsystems also in radio frequency (RF)-electronics. Perhaps the most well-known such applications are different kinds of mechanical switches [2-5], some of which have already been brought in to commercial use by companies such as TeraVicta and MagFusion [6,7]. Another commercially successful microfabricated device is the FBAR-filter [8] that can be found inside the mobile phones nowadays. Micromachined inductors and tunable capacitors as well as mechanical switches have been applied for phase-shifters, reconfigurable antennas and in beam steering [9-12] and in the resonant mode also as references in oscillator applications [13-15,29]. Also devices that are based on the mechanical resonance have been proposed for high precision frequency references [P1,37-44] and even for applications in signal processing like filtering [16,17]. The first commercial applications of MEMS-oscillators based on mechanical silicon resonators have been launched by companies such as SiTime and Discera [18,19], but the quality of those devices is not enough for frequency reference use and they are aimed for clock generation at different consumer and industrial markets. In addition to realizing existing functions with MEMS components and devices, MEMS can also be seen as an enabling technology; novel components like resonators combining mechanical frequency mixing and filtering [20-23,P3,P7] and mechanical, slow-velocity delay lines [24] have been realised. In turn, these devices have led to even new radio architectures [25,32].

This thesis presents new scientific findings in the field of high-frequency micromechanical devices. In this thesis special attention is paid on frequency reference and frequency conversion applications and especially on their stability and performance. As most of the work is performed with devices utilising mechanical resonances, Chapter 1 introduces the necessary background and mathematical models. Chapter 2 concentrates on issues concerning the stability of the MEMS devices – this is divided into short term stability (phase noise) and long-term stability (drift). It is shown that by using MEMS resonators, even strict GSM specifications can be met. Chapter 3 is dedicated to studying potential realisations for effective conversion of GHz-range communication signals down to the resonance frequency of the MEMS devices. The chapter presents a micromechanical mixer-filter ("mixler"). The performance of the mixler is characterised and further improvements are presented. Chapter 4 presents a process for fast prototyping of MEMS devices for research purposes. Finally, conclusions and future prospects are presented in Chapter 5.

1.1 Micromechanical resonator as both mechanical and electrical device

1.1.1 Linear resonator

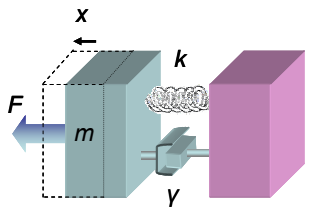

Fig. 1 Spring-mass system.

A micromechanical resonator can be represented as a spring-mass –system (Fig. 1) with an equation of motion

$$m\ddot{x} + \gamma\dot{x} + kx = F\,, \tag{1.1}$$

where m and k are the effective mass and the spring constant of the resonator, respectively and γ and F the damping constant and the external force acting on the system, respectively. With zero damping the eigenfrequency of the first fundamental mode can be written as

$$\omega_0 = \sqrt{\frac{k}{m}} \tag{1.2}$$

and the quality factor

$$Q \approx \frac{m\omega_0}{\gamma} = \frac{\sqrt{km}}{\gamma}. \tag{1.3}$$

With Eqs. (1.2) and (1.3) Eq. (1.1) can be written as

$$m\ddot{x} + \frac{m\omega_0}{Q}\dot{x} + kx = F\,. \tag{1.4}$$

Eqs. (1.1) - (1.4) are valid for small displacements x, *i.e.* in the linear region. For practical use the linear model has very limited use, this is the case especially with micromechanical devices in which the displacement amplitude can become significant when compared with other device dimensions as can be seen in the next chapter.

1.1.2 Nonlinearities

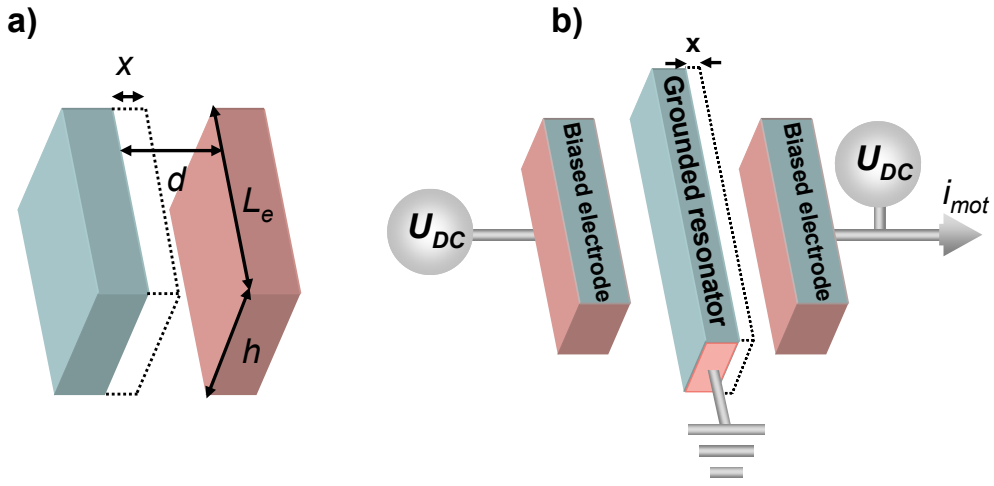

Fig. 2 a) Micromechanical capacitor and b) symmetrically biased resonator.

When a voltage difference U is applied between the two plates in Fig. 2, the energy in the capacitor stored between these two plates is

$$E = \frac{1}{2} C U^2, \tag{1.5}$$

where the C is the capacitance of the device ($C = L_e \times h \times \varepsilon_0/d$). If the biasing voltage is static $U = U_{DC}$, the moving plate experiences a force according to

$$F = \frac{\partial E}{\partial x} = \frac{U^2}{2} \frac{\partial C}{\partial x}. \tag{1.6}$$

The quadratic force-voltage relation in Eq. (1.6) is usually the most significant non-linearity that exists in capacitively coupled micromechanical devices.

While Eq. (1.6) is valid in the whole displacement amplitude range x, the other type of non-linear contributions become meaningful with increasing the displacement amplitude. They can, however, be included into Eq. (1.1) by replacing the linear spring constant with a non-linear one as

$$kx \rightarrow k_1 x + k_2 x^2 + k_3 x^3 + \ldots, \tag{1.7}$$

where the terms of the spring constant consist of both mechanical and electrical spring constants ($k_n = k_{mn} + k_{en}$). The higher order terms of the spring constant, k_n, can be either positive or negative and thus change the resonance curve to reflect hysteresis [26]. Also the first order spring-constant k_1 can be higher or lower than the linear spring constant k leading to either higher or lower resonance frequency, respectively.

Besides the force-voltage non-linearity that is depicted in Eq. (1.6) the capacitive coupling generates the capacitive non-linearity that is a common source for the non-linearity of the spring constant. For capacitive devices with plate transducers (Fig. 2 a) the coupling capacitance depends on the displacement amplitude, x, in a nonlinear way according to

$$C = \frac{A\varepsilon_0}{d - x} = \frac{L_e h \varepsilon_0}{d - x} = \frac{C_0}{\left(1 - x/d\right)}, \tag{1.8}$$

where L_e and h are the length and height of the transducer electrode, respectively and d is the coupling gap when the voltage across it is zero (Fig. 2). $C_0 = L_e \times h \times \varepsilon_0/d$ is the capacitance of the transducer at rest, *i.e.* when $x = 0$. If the displacement x is small when compared with the length of d the gradient in Eq. (1.6) can be linearised by writing $dC/dx \approx C_0/d$, but with increasing displacement higher order terms must be taken into account

$$\frac{dC}{dx} \approx \frac{C_0}{d}\left[1 + 2\left(\frac{x}{d}\right) + 3\left(\frac{x}{d}\right)^2 + 4\left(\frac{x}{d}\right)^3 + \ldots\right]. \tag{1.9}$$

When the capacitive non-linearity is introduced, the force Eq. (1.6) becomes

$$F \approx \frac{U^2}{2} \frac{C_0}{d}\left[1 + 2\left(\frac{x}{d}\right) + 3\left(\frac{x}{d}\right)^2 + 4\left(\frac{x}{d}\right)^3 + \ldots\right], \tag{1.10}$$

which can also be written as

$$F \approx \frac{U^2}{2}\frac{C_0}{d} + k_e x + \frac{3}{2}k_{e2}x^2 + 2k_{e3}x^3 + \ldots, \tag{1.11}$$

where

$$k_{en} = \frac{(n+1)}{2}\frac{C_0 U_{DC}^2}{d^{(n+1)}} \tag{1.12}$$

is the electrical spring constant of *n*th order. If the biasing is symmetric (Fig. 2 b) even order terms cancel each other and only the odd order terms are left. Therefore it is clear that the first order effect of the capacitive non-linearity is the reduction of the total spring-constant ($k \rightarrow k - k_e$) and due to that the decrease of the resonance frequency. As an approximation for the frequency change we may write the first eigenfrequency in Eq. (1.2) with the first order electrical spring constant

$$\omega = \omega_0\sqrt{1 - k_e/k_m} = \omega_0\sqrt{1 - \frac{C_0 U_{Dc}^2}{k_m d^2}} \approx \omega_0\left(1 - \frac{C_0 U_{Dc}^2}{k_m d^2}\right), \tag{1.13}$$

where km is the mechanical spring constant. the last approximation of Eq. (1.13) holds for small values of k_e.

Eventually the capacitive non-linearity will introduce a point of bifurcation where the transmission signal shows discontinuity and the oscillator trajectory depends on the initial conditions. This point of bifurcation sets the maximum vibration amplitude of the resonator called the *critical amplitude,* x_c [27]

$$x_c = \frac{2}{\sqrt{3\sqrt{3}Q|\kappa|}}, \tag{1.14}$$

where κ gives the amount of frequency shift due to the non-linear terms as

$$\omega = \omega_0\left(1 + \kappa x^2\right) \tag{1.15}$$

and is given by

$$\kappa = \frac{3}{8}k_2 - \frac{5}{12}k_1^2 \tag{1.16}$$

For oscillator applications, the critical amplitude sets the absolute maximum for the vibration amplitude and consequently for the mechanical energy.

On the other hand, the output current for a system in Fig. 2 b) can be expressed as

$$i_{mot} = \frac{dQ}{dt} = U_{Dc}\frac{\partial C}{\partial t} = U_{Dc}\frac{\partial C}{\partial x}\frac{\partial x}{\partial t} = U_{DC}\frac{C_0}{d}\left(1 + 2\frac{x}{d} + 3\left(\frac{x}{d}\right)^2 + \ldots\right)\frac{\partial x}{\partial t}, \quad (1.17)$$

where the term $U_{DC}(dC/dx)$ can be written as electromechanical coupling constant η. From Eq. (1.17) it is clear that even linear vibrational mode can result in higher harmonics and in the motional current. Therefore, for practical purposes only of the order of 10% of the critical amplitude is commonly used.

Besides capacitive non-linearity the critical amplitude can also be limited by the mechanical non-linear dependence. However, for the devices with high electromechanical coupling the amplitude range where the dependence is still linear is a few times the amplitude allowed by the capacitive non-linearity.

From Eq. (1.12) it is evident, that the electric field which is generated by the applied bias-voltage U_{DC} can be used to tune the spring constant of the resonator. This opens at least two options: i) by applying a constant voltage ($U = U_{DC}$) the resonant frequency of the resonator can be tuned and ii) by applying a periodically changing voltage ($U = u_{ac}$), the spring constant can be modulated, this can be used to realise a parametric amplification scheme as is shown in Chapter 3.3. Additional effects caused by the capacitive non-linearity will be discussed in Chapter 3.2.

1.1.3 Selected resonator designs

The resonators used in this thesis are the result of nearly ten years of research and development work. From the initial goal of reaching high-Q and very high resonance frequency ($f_{res} \approx 1$ GHz) the target was refined into a high-Q and high frequency ($f_{res} \approx 13$ MHz) resonator that is capable of producing strong output signal with excellent short- and long-term stability. In addition, experiments have been performed with multi-resonant structures that feature good frequency tunability. Fig. 3 shows some of the designs that have been designed and tested during the research period.

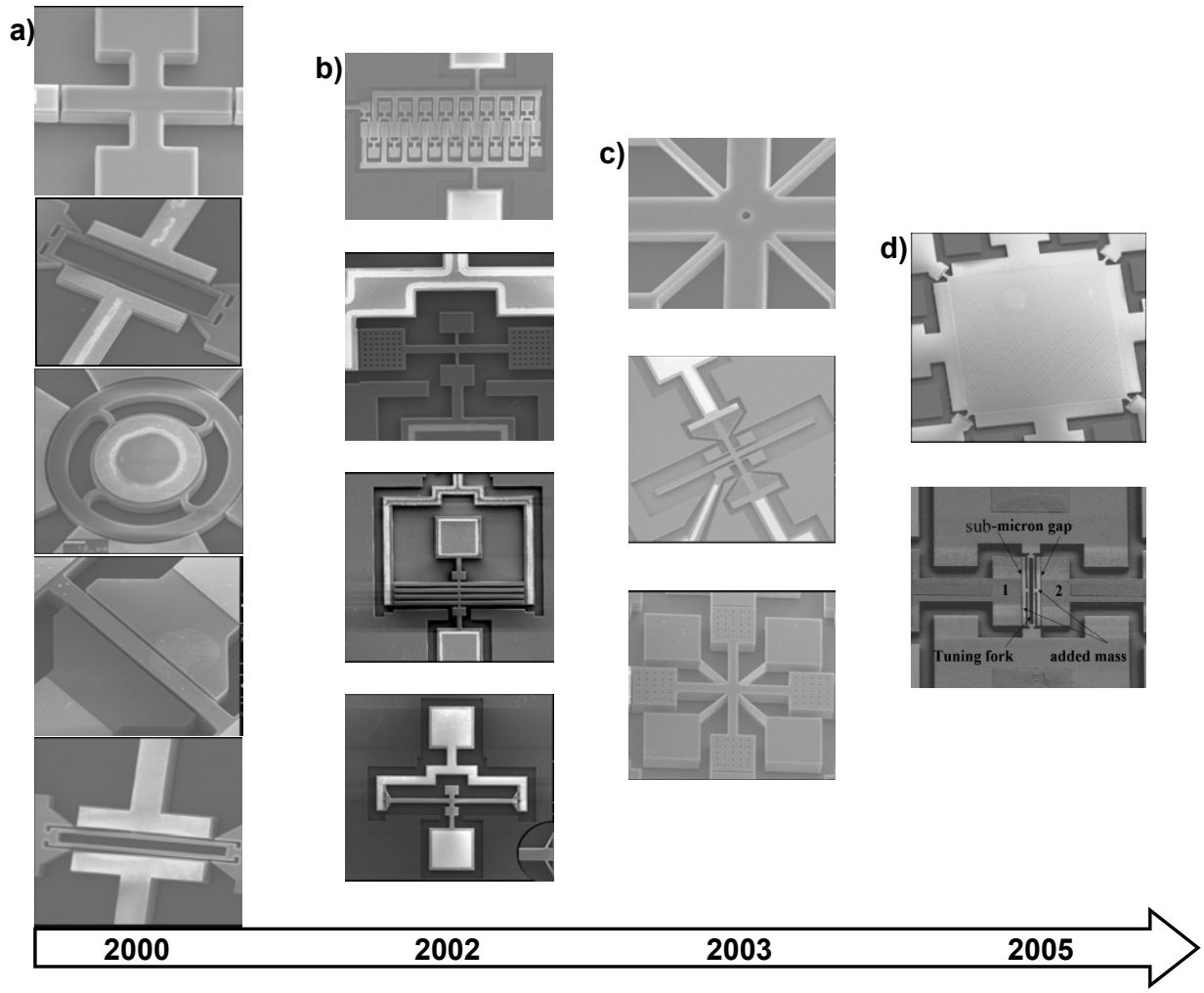

Fig. 3 Various resonators that were designed, fabricated and used in this thesis. The timeline in years goes from left to right depicting the current research interests at different points of the research: a) Testing of different concepts. (See for example [39,40].) b) Improving the electromechanical coupling and the Q-factor. (See for example [111,112]) c) Targeting towards the long-term stability. d) Current state of the art: high Q-factor, high energy resonators with narrow coupling gaps. All the depicted resonators have been developed and fabricated in collaboration with VTT – Technical Research Centre of Finland.

In this thesis three different resonator types are mainly used (Fig. 4). Two of the resonators feature the bulk acoustic vibration mode that results in very high Q-factors $Q_{2D} = 130\,000$ and $Q_{1D} = 180\,000$ in vacuum for 2D BAW (Fig. 4 a) and 1D BAW (Fig. 4 b), respectively, high mechanical spring constants k and moderate coupling gaps $d_{2D} = 0.75$ µm and $d_{1D} = 1$ µm. The Double-Ended-Tuning-Fork (DETF) (Fig. 4 c) shows a lower Q-factor and mechanical spring constant making the device not suitable for frequency reference applications, but a tempting alternative for studying the effects of capacitive non-linearity due to the high electromechanical coupling due to the narrow coupling gap of $d_{DETF} = 170$ nm.

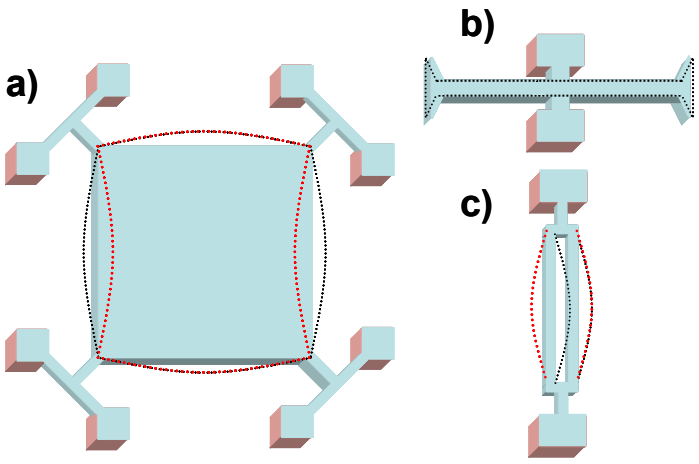

Fig. 4 Resonators used in this thesis and the relevant vibration modes (black and red dotted lines) a) Square-Extensional Bulk-Acoustic-Wave (SE-BAW or 2D BAW), where the used vibration modes are the Lame-mode (red) where the orthogonal edges vibrate in anti-phase and the SE-mode (black) where the orthogonal edges vibrate in phase. b) BAW (1D BAW) with a single length-extensional eigenmode. c) Double-ended-tuning-fork (DETF) with two used eigenmodes, one where the beams vibrate in-phase (black) and one where they vibrate in anti-phase (red).

1.1.4 Electrical equivalent circuit

When the resonator is displaced from the equilibrium position (Fig. 2 b) the motional current generated by the displacement Eq. (1.17) can also be written as

$$i = \frac{dQ}{dt} = \frac{\partial(CU)}{\partial t} = U\frac{\partial C}{\partial t} = U\frac{\partial C}{\partial x}\frac{\partial x}{\partial t} = U\frac{\partial C}{\partial x}\dot{x} = \eta\dot{x}. \tag{1.18}$$

Eq. (1.18) illustrates the transduction between the mechanical and electrical domains. Due to this reason η is sometimes called the transduction factor. As the MEMS devices are usually coupled to an electric circuit it is convenient to present the mechanical device with electrical equivalent components. This is a commonly used method in studying for example quartz crystals [28]. When a MEMS-resonator in Fig. 2 b) is represented by an equivalent circuit of Fig. 5, the electrical components can be estimated by comparing the differential equation of motion of the mechanical resonator with the respective equation of current in the electrical RLC-resonator

$$L\dot{i}(t) + Ri(t) + \frac{1}{C}\int i(t)dt = u(t) \tag{1.19}$$

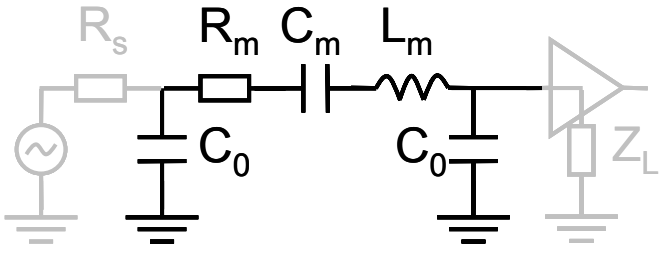

Fig. 5 Electrical equivalent circuit of a resonator in Fig. 2 b). The shaded parts represent the voltage source that is used to excite the vibration and the amplifier that is used to detect the actual resonance signal.

For another comparison one can to insert Eq. (1.18) into Eq. (1.1) and divide the result with the transduction factor η. Physically this mathematical operation means the conversion from force into voltage. The resulting equation for the mechanical resonator is

$$\frac{m}{\eta^2}\dot{i}(t)+\frac{\gamma}{\eta^2}i(t)+\frac{k}{\eta^2}\int i dt = u(t). \tag{1.20}$$

Now by comparing Eqs. (1.19) and (1.20), the equivalent component values can be observed to be

$$R_m = \frac{\gamma}{\eta^2} \text{ or } R_m = \frac{\sqrt{km}}{Q\eta^2}, \tag{1.21 a}$$

$$L_m = \frac{m}{\eta^2}, \tag{1.21 b}$$

$$C_m = \frac{\eta^2}{k} \tag{1.21 c}$$

1.2 Aim of the work

The purpose of the thesis is to contribute to the miniaturisation of microelectronics by studying the issues related to the stability and applicability of micromechanical resonators where conventionally macroscopic devices (for example quartz-crystals in frequency references and diode-rings in frequency mixers) are used. The thesis presents studies on issues that seek answers to the following points:

I Can MEMS-resonators be used to realize a high-precision frequency reference?
II How can one characterize physical factors contributing to the stability of MEMS-devices, including built-in –potentials?
III How effective is a microelectromechanical resonator as a frequency mixer and how one can improve its performance?
IV Is there a fast, simplified way to fabricate at least a few RF-MEMS components?

2 Micromechanical resonators as frequency references

An electrical frequency reference is a necessary component in practically any wireless transceiver. The stand-alone reference is needed especially in portable devices for establishing communication after power-up. During the last decade, one major goal in the field of MEMS has been to realise a reference oscillator that is able to compete with a frequency reference that is realised with a quartz crystal and that is able to fulfil the strict specifications needed in modern wireless communication. Under the most intense study have been the spectral purity (= short term stability), stability of the output frequency (= long term stability) and the power consumption.

MEMS-oscillators can be divided into two categories: i) oscillators that have their frequency base in microfabricated mechanical resonators and ii) oscillators that have their frequency base in microfabricated inductors and capacitors. For the sake of compactness only the former are discussed here, even though some interesting high-frequency oscillators have been realized using the latter approach [13-15,29]. Oscillators realised using MEMS inductors and capacitors usually feature higher frequency and larger tuning range when compared with the ones realised with mechanical resonators, but exhibit higher power consumption and worse phase-noise due to the lower achievable Q-factor. The mechanical resonators can be divided by their actuation and detection mechanisms into at least magnetostrictive [30], thermal [85], electromagnetic [31], piezoelectric and capacitive devices, of which the last two have shown some potential for high-precision oscillator applications. The piezoelectric oscillators include for example FBAR (Thin-Film Bulk Acoustic Resonator) [32].

2.1 Short-term stability

The short term stability dictates the spectral purity of the signal. It is usually specified through the phase-noise referenced at carrier power at certain offset from the carrier frequency (Fig. 6). For example in order to meet the GSM-specifications [48] for the receiver sensitivity and blocking, a 13 MHz reference oscillator must meet the phase noise specifications $\mathcal{L}_f$ = -130 dBc/Hz at Δf =1 kHz offset from the carrier and $\mathcal{L}$ = -150 dBc/Hz far away from the carrier (so called noise floor) [P1]. The strict phase-noise requirements arise from the fact that for practical use the output frequency of an oscillator is multiplied in a phase-locked loop (PLL) to match the carrier frequency (e.g. 900 MHz for GSM-900) and naturally the existing low-frequency noise becomes multiplied in a same process.

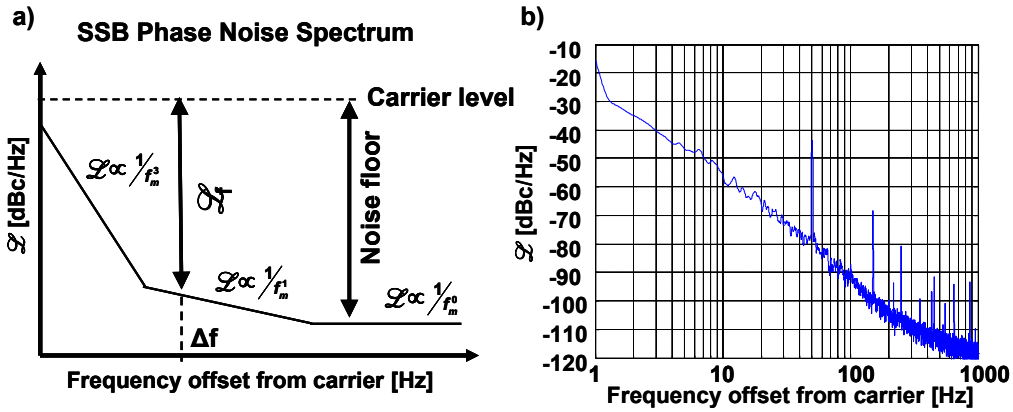

Fig. 6 a) Definition of SSB (single-side-band) noise. b) Actual measured phase-noise of an SE-BAW oscillator [41].

Typically the single-sideband phase noise-to-carrier ratio for an ideal oscillator can be approximated by Leeson's equation [33,34]

$$\mathscr{L}(\Delta\omega) = \frac{1}{4\pi}\frac{k_b T}{E_{vib}}\left(\frac{\omega_0}{Q\Delta\omega}\right)^2, \tag{2.1}$$

from which two important factors can be seen: i) in practice the phase-noise reflects the competition between the mechanical energy E_{vib} of the resonator and thermal noise k_bT and ii) the width of the resonance ($1/Q$) leads to a band-pass filtering of the noise reducing the noise as the frequency difference to the carrier $\Delta\omega$ increases. From Eq. (2.1) it seems that a usual direct comparison between a macroscopic quartz-crystal and microscopic silicon resonator in terms of phase-noise is not a fair one due to the orders of magnitude different resonator volumes. However, the 2D BAW silicon resonator allows nearly two orders of magnitude higher energy per volume ratio than quartz resonators (1.8×10^5 J/m^3 vs. 190 J/m^3) [27].

In a more generic form of Eq. (2.1) the noise voltage includes also the noise contribution from the amplifier electronics.

$$\mathscr{L}(\Delta\omega) = \frac{|u_n|^2}{|u_{ac}|^2}\left[\left(\frac{\omega_0}{2Q\Delta\omega}\right)^2 + 1\right], \tag{2.2}$$

where u_{ac} is the signal voltage which is usually limited by the non-linearities of the reference component (i.e. MEMS resonator) and u_n is the total noise voltage. However, for capacitively coupled devices Eq. (2.2) does not take into account the effect of aliasing of the *1/f* noise due to the capacitive coupling. In the capacitive transduction gap, the *1/f* noise is mixed with the signal voltage produced by the resonator giving an additional noise term. A more accurate equation for the dual side-band noise has been presented by Kaajakari *et. al.* [35] as

$$\mathscr{L}(\Delta\omega) = \frac{|u_n|^2}{|u_{ac}|^2}\left[\left(\frac{\omega_0}{2Q\Delta\omega}\right)^2 \cdot \left(1 + 2|\Gamma|^2 R_m^2 |u_{ac}|^2 \frac{\omega_c}{\Delta\omega}\right) + 1\right], \tag{2.3}$$

which leads to Eq. (2.2) with a aliasing factor $\Gamma = 0$. It can be seen from Eq. (2.3) that the phase noise will decrease as $1/\omega^3$. The noise is divided by a factor of two to take into account only the actual phase noise, not the amplitude noise. As can be seen from all Equations (2.1) - (2.3), a high quality-factor of the resonance lowers the phase-noise. However, this is not the whole truth as the high quality factor also reduces the maximum linear vibration amplitude of the resonator Eq. (1.14). It is evident from Eq. (2.3) that increasing the vibration amplitude does not help with aliasing of *1/f* noise when it comes to the noise that is very close to the carrier frequency as it is produced by the mixing of the thermal noise and the signal produced by the resonator. However, the noise floor becomes lower by increasing the vibration energy of the resonator. In order to improve the near carrier noise, it is important to optimize the noise performance of the sustaining amplifier and aim for low mechanical equivalent resistance, R_m.

2.1.1 Published low phase-noise oscillators

[P1] presents an oscillator that is based on an Square-Extensional Bulk-Acoustic-Wave (SE-BAW) resonator (Fig. 4 a) [36]. The resonator is optimized for both the high quality factor and sufficient energy-storage in order to realize a low phase noise oscillator. It is the first MEMS-resonator based oscillator capable of meeting the GSM-specifications with respect to phase noise. The measured figures are $\mathscr{L}_f$ = -138 dBc/Hz at Δf = 1 kHz offset from 13 MHz carrier and noise floor far from the carrier frequency is $\mathscr{L}$ = -150 dBc/Hz. For comparison, Table I lists some published oscillators that are based on MEMS-resonators.

Table I – Low phase-noise oscillators realized with MEMS-resonators

Used resonator (published)	$\mathscr{L}_f$ at 1 kHz [dBc / Hz]	$\mathscr{L}$ [dBc / Hz]	Frequency [MHz]	Q [$\times 10^3$]	Vibration mode	Comments
SE-BAW [P1,37] (2004)	-138	-150	13	130	2D volume expansion	Discrete amplifier[1]
c-c[2] beam [38] (2001)	-80	-115	9.75	3.6	Flexural/ bending	Discrete amplifier
c-c[2] beam [39] (2002)	-105	-120	14	1.5	Flexural/ bending	Discrete amplifier[1]
1D-BAW[40] (2002)	-115	-120	12	180	1D length extension	Discrete amplifier[1]
SE-BAW [41] (2005)	-130	-147	13	130	2D volume expansion	Wirebond to 0.35 μm CMOS, P_c = 240 μW
Wine-glass [42] (2004)	-110[3]	-132[3]	60	145	2D volume expansion	P_c = 780 μW
Array of wine-glass [43] (2005)	-123[3]	-136[3]	60	119	2D volume expansion – 9 parallel resonators	With TSMC 0.35 μm CMOS P_c = 350 μW.
Quartz-crystal TCO-9141	-141	<150[4]	13-26	300[4]	Shear mode	P_c = 6 mW[4].

[1] Philips BF545B JFET at input
[2] Clamped-clamped or bridge resonator
[3] -15 dB if scaled to f_{osc} = 10 MHz output frequency
[4] Estimate

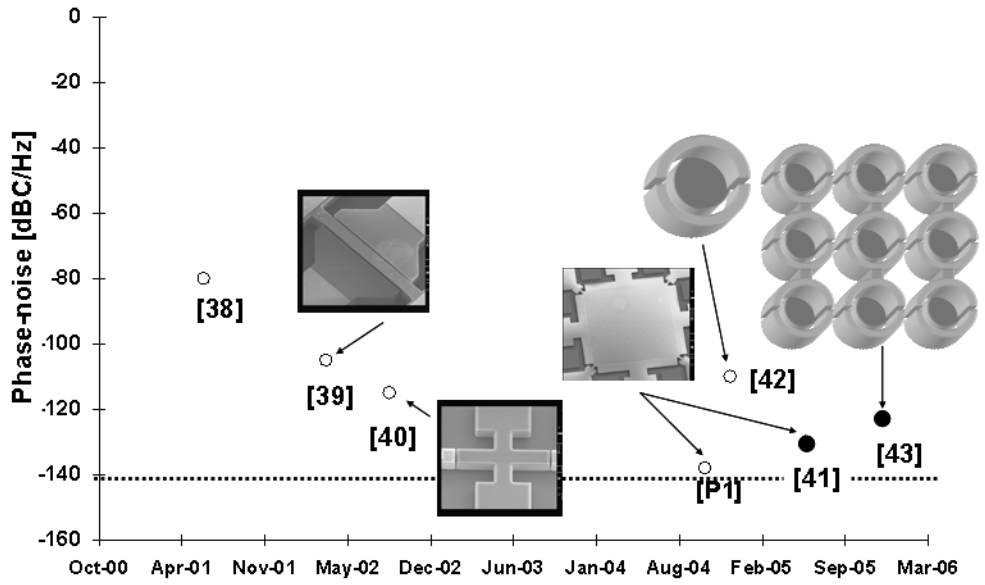

Fig. 7 Phase-noise of different micromechanical oscillators. The phase-noise has been normalised to f_{osc} = 10 MHz output frequency. The solid circles indicate the oscillators that were realised with integrated electronics. The dotted line marks the phase-noise of a commercial quartz-oscillator (TCO-9141). Note that the resonator images are not to scale.

From Table I and Fig. 7 it is evident that silicon micromechanical oscillators can compete with quartz crystal based reference oscillators and can be used to realise excellent reference oscillators *when it comes to short-term stability*. As already mentioned the key properties when realising an oscillator with low phase-noise are the sufficient energy storage that can be achieved in resonators with large volume and volume-expansion mode, and high Q-factor. In addition, due to the aliasing of 1/*f* noise, it is also important to optimize the amplifier for low frequency noise performance [35,44]. It is evident from Table I that a significant advantage of micromechanical oscillators is over an order of magnitude lower power consumption with a comparable phase-noise performance to macroscopic quartz oscillators.

2.2 Long-term stability

In addition to short-term stability also good enough long-term stability is required in frequency reference applications. The long-term stability for various applications is usually specified by studying the drift of the centre frequency. When this drift is known, a potential lifetime of the reference can be deduced. Table II shows the centre frequency stability requirements for various applications.

Table II – Centre frequency accuracy for various wireless applications

Application	Requirement $\Delta f/f$
Low data-rate (eg. Zigbee)	± 40 ppm [45]
High data-rate (eg. UWB)	± 25 ppm [46]
Bluetooth	± 30 ppm [47]
GSM	± 1 ppm [48]

When the long-term stability is discussed, usually the terms aging and drift are used. A*ging* is defined as the systematic change in frequency with time due to internal changes of the oscillator, when the external factors (e.g. temperature and humidity) are kept constant [49]. Aging is usually caused by changes of the device material due to the cracks, stress or strain and diffusion. This topic has been reviewed thoroughly for example by Vig *et al.* [50]. By [49] *drift* is defined as systematic change in frequency with time. This means that drift includes aging and the effects of changing external factors (e.g. temperature and pressure).

In order to realise a frequency reference with sufficient stability the ideal stability of the resonator must be known. This requires studying of the aging of the resonator. In order to characterise this effect, the external factors contributing to the resonance frequency must be eliminated or their effect compensated. Early studies [51] suggested that the stability of the MEMS-resonators would be insufficient for many frequency reference applications, but from those days the resonator designs have been improved. In the following Chapters, various factors contributing to the stability of MEMS-resonators are reviewed.

2.2.1 Effect of temperature on the frequency stability of MEMS

Perhaps the most well known cause for instability for the MEMS-resonators made out of silicon is the change of the resonance frequency with respect to temperature. Unlike quartz-crystals that can be fabricated so that the temperature has a minimum effect on the frequency of the resonator for a certain range of temperature (for example AT-cut [28]) silicon resonators always exhibit a temperature drift. This is due to the fact that the dependence of the temperature of all the elastic coefficients of the Young's modulus are of the same sign [52]. Fig. 8 shows a typical behaviour for a square-extensional (SE) mode microresonator [53] that shows a temperature dependence of the frequency ($(\Delta f/f)/\Delta T$) ≈ -30 ppm/K for both eigenmodes. The large negative frequency-temperature coefficient of silicon can be reduced by coating the resonators with dielectric layers like SiO_2 [54] or Al_2O_3 [55] that have a positive temperature coefficient of the frequency. However, thin films are usually amorphous meaning that this treatment may affect the quality factor and degrade the long-term stability. The layers are also susceptible to dielectric charging that can further reduce the long-term stability. Also, the resulting frequency-temperature coefficient may vary from device to device reducing the systematic predictability of the temperature dependence.

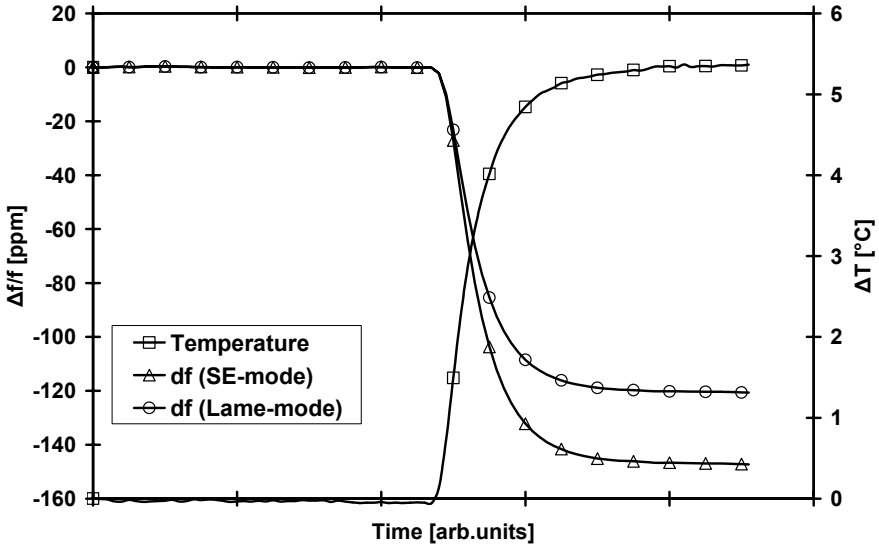

Fig. 8 Change in the resonance frequency of two vibrational modes of an SE-BAW MEMS-resonator with respect to the temperature.

When considering aging, the effect of temperature as an external instability source should be minimised or compensated by placing the devices into a temperature controlled chamber or by measuring the temperature and removing mathematically its effect from the measured data. On the other hand, when realising a frequency reference, actual temperature compensation must be done – the compensation can be either intrinsic [56] or it can be based on measuring the temperature and using this information to correct for the temperature induced drift for example with the aid of a tunable PLL [54,57]. Temperature compensation of the MEMS-based frequency references is a field of study that has only lately started to gain wider attention.

If the compensation is not intrinsic but is based on the measured temperature of the resonator it is important that the thermal contact with the sensor and the resonator is as good as possible to avoid any transient hysteresis. The optimum would be to measure the temperature directly using the resonator itself. Fig. 9 shows an example where the temperature measurement is based on measuring the change of the resonance frequencies of the two eigenmodes of on SE-BAW resonator. The temperature is deduced with the aid of known temperature coefficients of the mechanical resonance frequency (so called 2-mode temperature measurement) [53]. To demonstrate the power of this approach in comparison with an external sensor, the output frequency of the resonator is mathematically compensated using the temperature information acquired by measuring the centre frequencies of the two resonances and by combining this and the temperature information from a Pt-100 temperature sensor that is placed in a thermal contact with the resonator chip. The output frequency compensated with the Pt-100 sensor shows a frequency error of $\Delta f/f \approx 15$ ppm due to the nonideal thermal equilibrium between the sensor and the resonator. However, when the the 2-mode measurement was used, the temperature drift of the frequency was kept below $\Delta f/f \ll 1$ ppm.

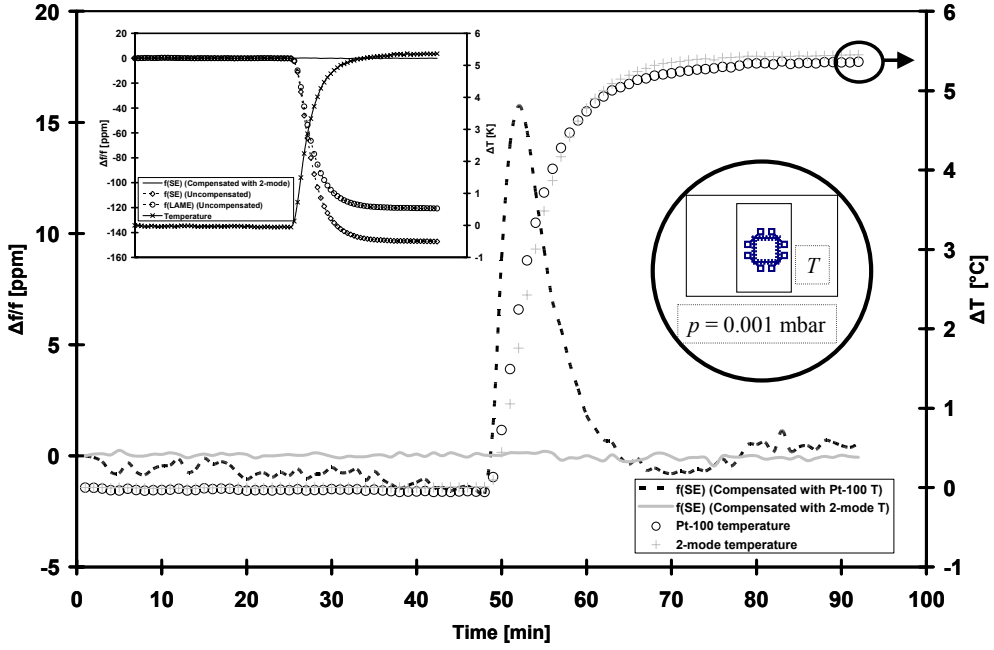

Fig. 9 The resonator was placed inside an environmental chamber and was subjected to a temperature ramp. The frequency shifts of the two eigenmodes were recorded (shown in inset) to deduce the temperature (crosses). This information was used to remove the effect of temperature on the resonance frequency of the SE-mode (solid line). As a comparison, the temperature was measured with an external Pt-100 sensor (circles) for removing its effect on the results (dashed line). The latter measurement clearly shows the thermal non-equilibrium between the sensor and the resonator during the temperature ramp [53].

2.2.2 Effect of mass change

As the resonance frequency of the resonator to is related its mass according to Eq. (1.2), it is clear that the change of the effective mass of the resonator changes also the frequency of the resonance. Mass can increase due to adsorption of contaminant molecules (e.g. water) onto the resonator surface or it can decrease due to outgassing (evaporation) of contaminants. In addition to molecular level adsorption, also larger particles can be adsorbed when the resonator is exposed to contaminated environment, one example being smoke [58]. Besides lowering the resonance frequency due to the mass increase, adsorption can also lead to stiffening of the resonator, in which case the resonance frequency is increased [58]. For frequency reference applications the change of the resonance frequency due to mass change is always harmful, but for other applications, like in the case of resonant sensors the mass-loading effect can be taken use of [see for example 59-61].

The humidity of the ambient air can also affect the resonance frequency through the mass loading effect, *i.e.* due to adsorption of water molecules onto the resonator surface. This was already shown in 1999 by van Arsdell *et al.* [62] in a study where the resonance frequency of a MEMS-resonator was monitored in dry air ($c_{H2O} < 10$ ppm) and in damp air with 50% and 75% relative humidity (RH). Their study showed that especially in case there are numerous cracks in the resonator, the increase in RH increased the drift of the resonance frequency. Humidity can be removed from the sample by heating [62,63] as shown in Fig. 10. However, when heating was stopped, the resonance frequency started again to decrease. Due to high power consumption required by the Joule heating, continuous heating is not usually a valid method to stabilise the resonator especially in low power applications. However, if this approach is selected, also the temperature drift can be removed as the resonator is constantly kept at a higher than the ambient temperature. This approach for temperature compensation is commonly applied in oven controlled high-precision crystal oscillators (OCXO).

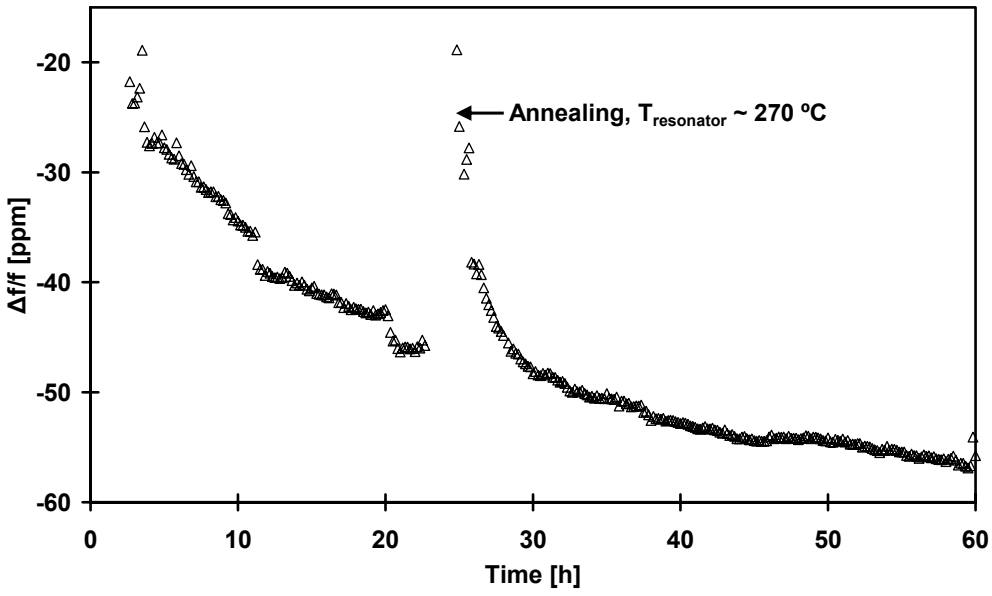

Fig. 10 Annealing the resonator for $t = 2$ h at $T = 270$ ºC resets the drift and releases adsorbed water from the surfaces.

2.2.3 Effect of bias-voltage change

Usually the bias-voltage of the resonators is assumed to be constant and not affecting the stability of the resonance frequency. However, to minimise the possible effect of drifting of the bias-voltage onto the resonance frequency it is convenient to select a resonator with large mechanical spring constant k_m as is suggested by Eq. (1.13). However, this naturally limits also the tunability of the resonator. On the other hand, to maximise the electromechanical coupling, it is convenient to have a gap as narrow as possible, but this in turn leads also to larger drift of the resonance frequency due to the bias-voltage drift. The sensitivity of the resonance frequency with respect to the small changes in the bias-voltage (i.e. noise) can be calculated estimated using a bias-voltage sensitivity factor, ψ, that can be derived by differentiating Eq. (1.13) with respect to the bias-voltage U_{DC}

$$\psi = \frac{C_0 U_{Dc}}{k_m d^2}\left(1 - \frac{C_0 U_{DC}^2}{k_m d^2}\right)^{-1/2}. \tag{2.4}$$

Eq. (2.4) has been divided by ω_0 to attain the relative change in the resonance frequency.

As an example we can calculate the required bias-voltage drift to change the resonance frequency for the devices in Fig. 4 a) and c) by 1 ppm. The results are shown in Table III.

Table III – Calculated effect of the bias-voltage drift on some of the resonators studied

	2D–BAW	2D–BAW	DETF
d [nm]	750	170	170
k_m [N/m]	14.5×10^6	14.5×10^6	166
C_0 [fF]	33	146	52
U_{DC} [V]	100	20	7
k_e @ U_{DC} [N/m]	587	2017	88
ψ [ppm/V]	4.0×10^{-1}	7.0	1.1×10^5
ΔU_{DC} to 1 ppm $\Delta f/f$	**2.44 V**	**144 mV**	**9 µV**

2.2.4 Long-term stability of MEMS-resonators

[P2] presents a study of the long-term stability of four identical micromechanical 1D BAW-resonators (Fig. 4 b). The resonators feature high quality factor (Q = 170 000 at p < 1 mbar and Q = 2 000 at p = 1 bar) and improved electromechanical coupling through triangle-shaped end points of the resonating arms. These factors ensure that the resonance is detectable even at normal atmospheric pressure. This allows the comparison between the vacuum encapsulated samples (encapsulating pressure p = 0.01 mbar and temperature T = 400 ˚C with residual pressure $p \approx 5$ mbar) with the ones that were operated under atmospheric humidity and pressure.

In [P2] the drift of a resonance frequency of encapsulated samples was compared with un-encapsulated samples in a temperature controlled environmental chamber with variable RH for a monitoring period of t = 1 000 h (~ 42 days). When the temperature induced change in the resonance frequency is removed with the aid of measured temperature and temperature coefficient ($(\Delta f/f)/\Delta T$) ≈ -28 ppm/K the effect of humidity is revealed in the resonance frequency drift of the un-encapsulated samples (Fig. 11). The calculated correlation factors between the relative humidity

and the resonance frequency of the un-encapsulated samples 3 and 4 are -0.88 and -0.85, respectively, indicating that the resonance frequency is significantly affected by the relative humidity.

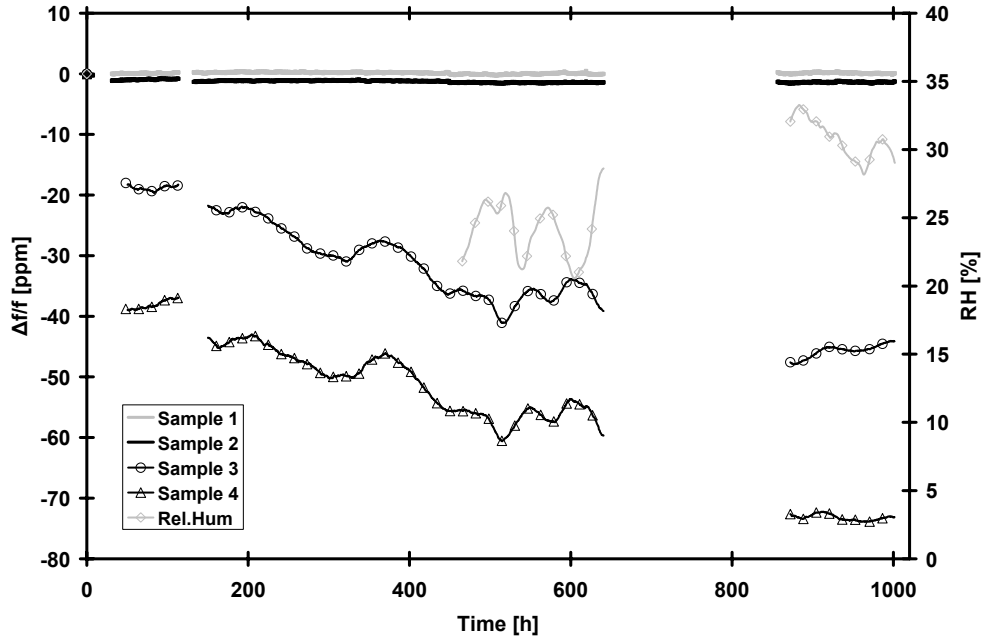

Fig. 11 The change of resonance frequency (*Δf/f*) of the four measured samples. Samples 1 and 2 are encapsulated and samples 3 and 4 are left open. The temperature-induced variations are removed from the data based on the recorded Pt-100-temperature and the measured temperature coefficient (*1/f×Δf/ΔT* ≈ -28 ppm/K). The axis on the right shows the measured ambient relative humidity.

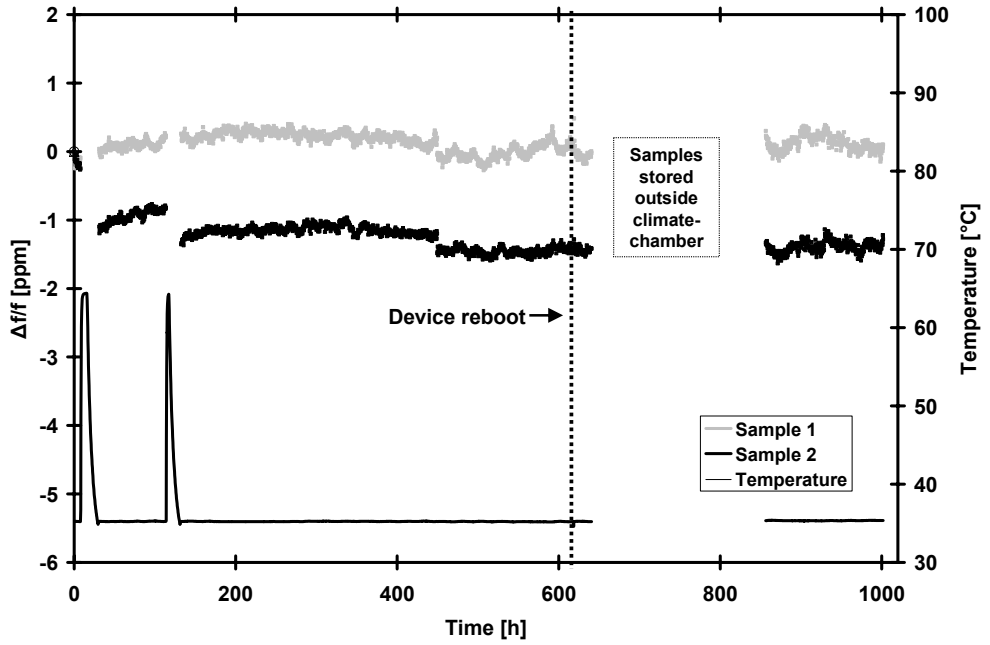

Fig. 12 The change of resonance frequency for the two encapsulated samples. The temperature-induced variations are removed from the data based on the recorded Pt-100-temperature (shown on the right-axis) and the measured temperature coefficient (*1/f×Δf/ΔT* ≈ -28 ppm/K).

When the samples are protected from ambient atmosphere and humidity, the drift of the resonance frequency is significantly lower (Fig. 12). Fig. 12 also shows that even a ppm level stability is achievable as long as the resonators are hermetically protected from the ambient atmosphere. The linear fits to the measured data of the packaged resonators show a drift of $\Delta f/\Delta t = -1.15\times10^{-4}$ Hz/h and $\Delta f/\Delta t = -5.25\times10^{-4}$ Hz/h for samples 1 and 2, respectively. While extrapolations to longer periods should always be treated with a certain suspicion, a drift of this degree would allow a ppm-level centre frequency accuracy for a period exceeding one year. Other published results concerning the long-term stability of silicon micromechanical resonators are collected in Table IV.

Table IV – Long term stability results.

Resonator	f_{res}	$\lvert\Delta f/f\rvert$ [ppm] / monitoring time	Comments
1D BAW [P2]	13 MHz	< 1 / 1 000 h	Encapsulated
1D BAW [P2]	13 MHz	75 / 1 000 h	Unencapsulated
2D BAW [64]	13 MHz	0.009 / month 0.03 / month	Encapsulated - Drift calculated as linear fit to measured data
Cf[1]-beam [64]	511 kHz	4.2 / month	Encapsulated - Drift calculated as linear fit to measured data
Flexural [65]	129 kHz	± 3.7 / 10 000 h	Wafer-scale film encapsulated
Flexural (DETF) [65]	155 kHz	± 3.1 / 10 000 h	Wafer-scale film encapsulated
Torsional [62]	45 kHz	± 45 / 20 h	Control sample (no pre-cracks)
		31 000 / 20 h	pre-cracked @ RH 75%
Torsional [66]	3-11 MHz	~ 150 / 200 h	Un-encapsulated, covered with C-teth SAM[2]
Torsional [66]	3-11 MHz	~ -100 / 200 h	Un-encapsulated, covered with Ox-teth SAM[2]
Torsional [66]	3-11 MHz	~ -500 / 200 h	Un-encapsulated with hydrogen terminated surface
Quartz-crystal (TCO-9141)	13-26 MHz	< ± 1 / year	Commercial reference oscillator.

[1] Clamped-free or singly clamped resonator
[2] Self-Assembled-Monolayer utilized to prevent water adsorption

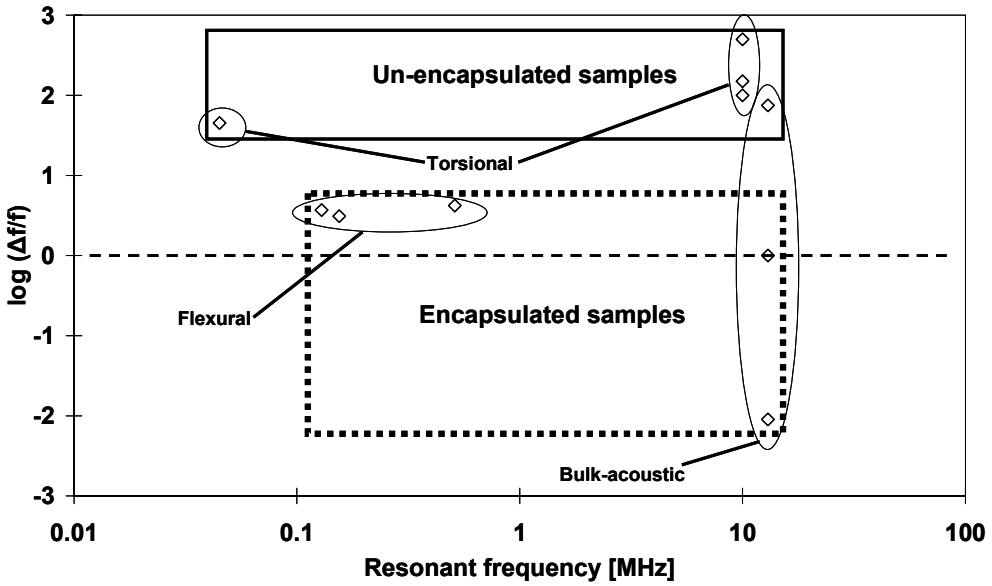

Fig. 13 Results from the long-term stability measurements from Table IV typically show the difference between the encapsulated and un-encapsulated samples. It should be noted, that the measurement times are not equal, however, it is evident that only the samples using bulk-acoustic volume modes show the long-term stability of $\Delta f/f \leq 1$ ppm (dashed line). On the other hand, even the bulk acoustic mode resonators have to be encapsulated to obtain this level of stability.

Measurements of the torsional samples reveal that proper surface treatment improves the stability but is not alone enough to stabilise the resonance frequency to meet the specifications for any practical frequency reference. On the other hand, as intrinsic silicon is very stable material, the hydrophobic coating can actually degrade the stability due to evaporation. In order to reach proper long-term stability a hermetic packaging is needed. It should also be noted that the resonator geometry and the mode of vibration play an important role when aiming at the maximised stability. As conclusion from Table IV and Fig. 13 it can be seen that it is possible to use capacitively coupled micromechanical resonators to realise a reference oscillator that fulfils the GSM specification in terms of *long-term stability* requirements of a reference oscillator.

2.3 Method to analyse built-in potential in MEMS devices

Another physical factor playing a role in the stability of various MEMS-devices is the built-in potential V_{bi}. Even though its origin is rather well known, the effect on the stability has been less studied. The built-in potential appears as an extra DC-voltage in capacitively coupled devices. A good example of the built-in potential in the case of capacitive accelerometer is shown in Fig. 14 [P5] where the built-in potential causes the displacement of the proof-mass even in the case of zero acceleration of the device. The built-in potential has also been seen to be a stability degrading phenomenon in the MEMS-based voltage-references [67,68] where some solutions have been found to minimise its effect [69]. For RF-MEMS switches the effect of built-in potential could become an issue in terms of change in the pull-in voltage, but can also lead to device stiction due to the charging of the dielectrics [70,81]. Similar effect takes place in MEMS-resonators where this voltage modifies the electric spring constant and thus changes the resonance frequency of the device as was shown in Chapter 2.2.3. The effect could be further increased if the coupling of the MEMS-devices is improved by introducing the dielectric layers in the coupling gap [71].The spontaneous

built-in voltage can also be useful, one such example is the vibrating power harvester system with built-in voltage [72].

Built-in voltages are generated when two dissimilar materials are brought into contact –it is in principle a direct measure of the difference in the work functions [73]. In practice, however, the observed work functions are modified due to the dielectrics present on the surfaces [74,75] and vary as a function of the temperature and due to the adsorbents on the surfaces [76,77]. Extensive studies on the built-in potential and its temperature dependence in capacitive accelerometers have shown that the measured values agree only partially with the theory [78,79] and that the variations can be significant even for identical samples fabricated on the same wafer. The latter observation is also visible from Fig. 16 b). Therefore for many practical cases experimental methods are needed to unambiguously determine the built-in potentials of the interfaces.

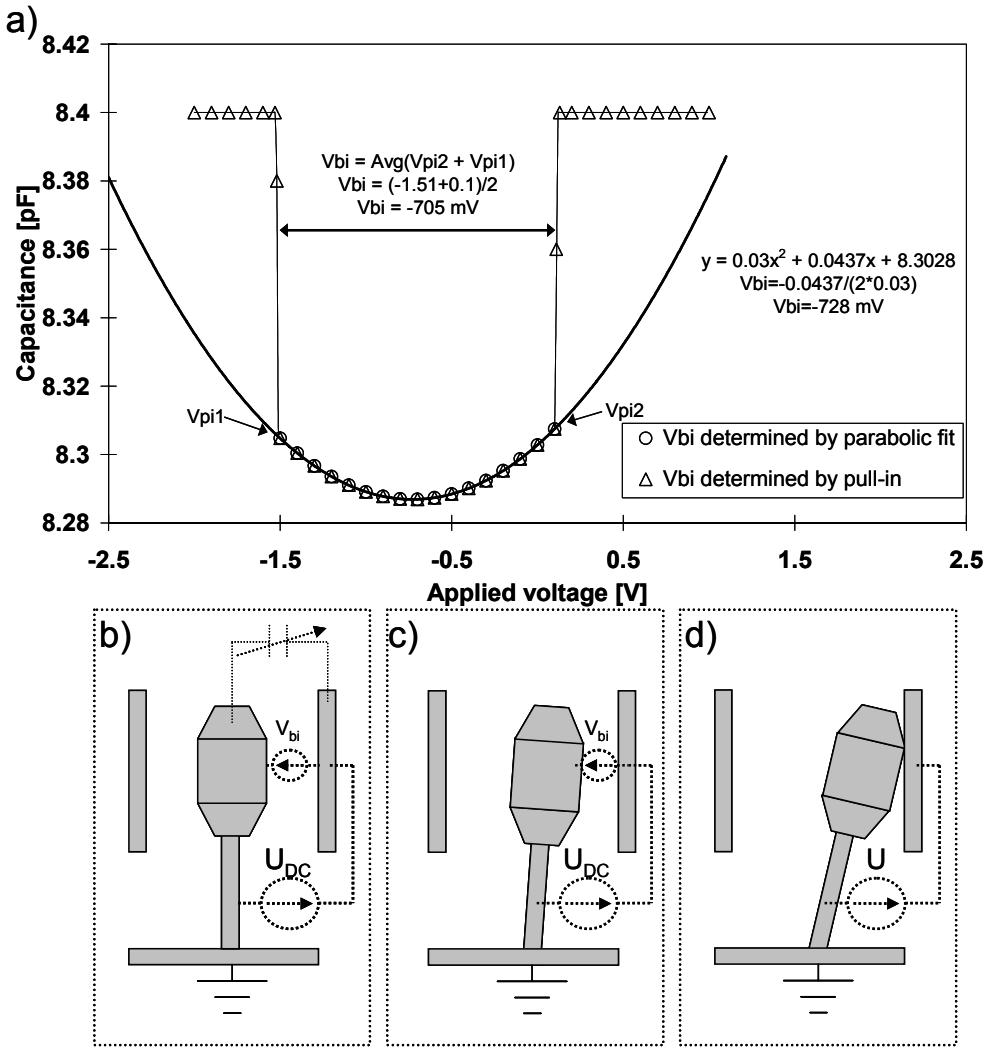

Fig. 14 a) In capacitive sensors the built-in potential manifests itself as a zero-point offset that can be observed by measuring the capacitance of the sensor as a function of applied bias-voltage U_{DC}. b) The capacitance is at minimum when $U_{DC} = -V_{bi}$. c) When $U_{DC} \neq -V_{bi}$ the capacitance increases due to the electrostatic force. d) When the voltage between the electrodes ($U = U_{DC} + V_{bi}$) exceeds the pull-in voltage, the electrostatic force draws the electrodes into contact [P5].

Publication [P5] presents a method to measure the built-in voltage inside closed cavity MEMS-devices. A capacitive device can be represented by a system of two electrodes, one movable and a

static one (Fig. 15). To make the situation more generic we can assume that there is a layer of dielectric on the static electrode and that the electrodes are fabricated from different materials with work functions φ_1 and φ_2 for static and movable electrodes, respectively. This kind of scheme applies well to any capacitive MEMS-sensor or for example electrostatically actuated resonator.

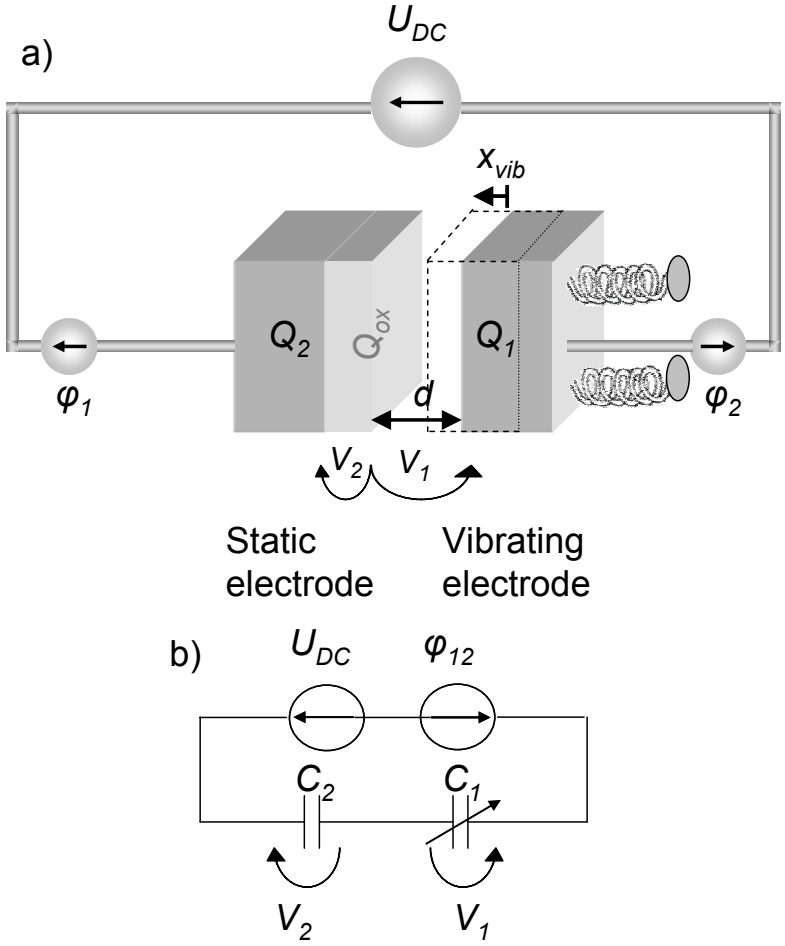

Fig. 15 a) Measurement scheme of the built-in voltages. b) Simplified electrical equivalent for the system. The symbols φ_1 and φ_2 refer to the work functions of the electrode materials.

When the movable electrode vibrates at frequency ω, the charges Q_1 and Q_2 are reallocated and the current generated was shown to be [P5]

$$i(t) = \frac{dQ_1}{dt} = -\frac{dQ_2}{dt} = \frac{-\alpha\beta\omega\cos(\omega t)(C_2(U_{DC} - \phi_{12}) - Q_{ox})}{((1+\beta\sin(\omega t)) + \alpha)^2}, \tag{2.4}$$

where α is defined as the ratio of the capacitances $\alpha = C_1/C_2$. Where C_1 is the initial capacitance over the air gap ($C_1 = \varepsilon_0 \times A/d$) and C_2 the capacitance over the dielectric ($C_2 = \varepsilon \times A/t_{ox}$). β is the relative vibration amplitude, $\beta = x/d$. The magnitude of the current at frequency ω in Eq. (2.4) is a linear function of the applied bias-voltage U_{DC} which becomes evident by writing an approximation of Eq. (2.4)

$$i(t) \approx -\alpha\beta\omega\cos(\omega t)\left[C_2\left(U_{DC} - \phi_{12}\right) - Q_{ox}\right] \times \left(\left[1 - \beta\sin(\omega t)\right] - \alpha\right)^2, \tag{2.5}$$

and by collecting the terms sharing the ω dependence. This is also depicted in Fig. 16 a).

The current in Eq. (2.4) becomes zero when the applied bias-voltage

$$U_{DC} = \phi_{12} + \frac{Q_{ox}}{C_2} = V_{bi}, \tag{2.6}$$

where V_{bi} is the *built-in voltage* of the system that acts as an additional bias-voltage. By using lock-in amplifier for generating the excitation signal and measuring the output with the aid of an operational amplifier, the built-in potential V_{bi} can easily be deduced from the zero crossing of the current - bias-voltage curve (Fig. 16 a).

The system was successfully tested for capacitive accelerometers with good accuracy as compared to slower capacitance-voltage (C-V) measurements (Fig. 16 b). The displacement was induced by a mechanical shaker. Especially for low-mass, stiff MEMS-resonators the mechanical shaker may not be able to generate the necessary movement. In this case the vibration may be generated through electrostatic force, but the voltage can lead to trapping of charges and change the actual built-in voltage [80,81].

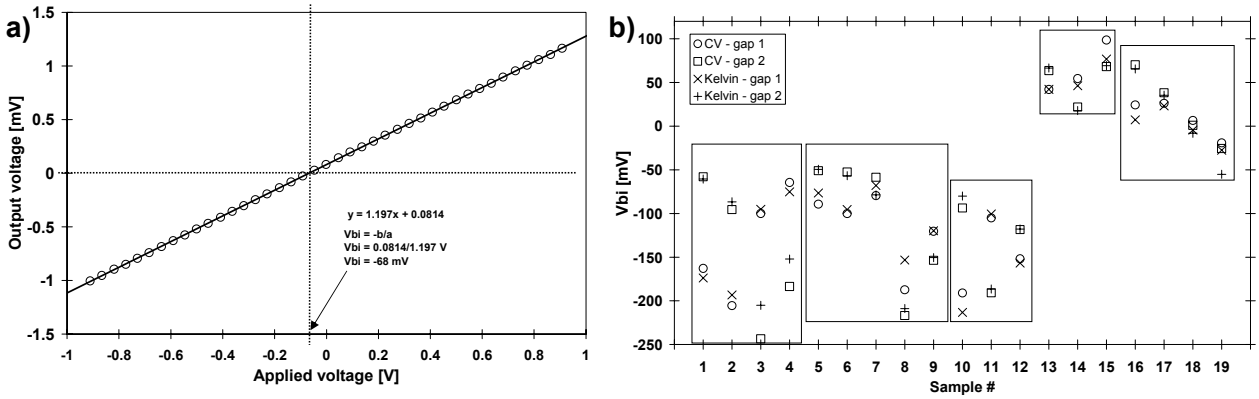

Fig. 16 a) Measurement result of an accelerometer shows the linear dependence of the output as a function of the applied bias-voltage and the built-in potential was deduced from the zero-crossing point of the output. b) Comparison of measured built-in potentials. The boxes indicate various groups of similar accelerometers. This illustrates some unpredictability in the built-in voltages. However, the results obtained with the C-V measurements (○ and □) and the results obtained with the method proposed in [P5] (× and +) agree well [P5].

3 Frequency conversion with MEMS-devices

Usually those silicon-based resonators that contain smallest features in the micrometer range possess mechanical resonances ranging from a few to few tens of MHz. This is appropriate for example in VCO (Voltage controlled oscillator) -applications, but for communication use the carrier signals used lie usually within the GHz-range. One way to facilitate the use of GHz-range signals is to use resonators that operate in the GHz-frequencies [82-84], but as the mechanical impedance of the resonators usually increases with decreasing size, the increase in frequency leads to a higher impedance level that is difficult to match for coupling. For this reason the first logical task in a MEMS-based transceiver is to convert the signal from high communication frequency to the resonance frequency of the MEMS-devices.

As the down-conversion is usually done with a mixer that performs a multiplication of the input signals it requires a nonlinear circuit. Conventional frequency mixers perform the mixing with the aid of diodes, transistors and transformers through the non-linearity in the voltage-current behaviour. The non-linearities (Chapter 1.1.2) of capacitive MEMS-resonators can also be used to perform the operation. As an added benefit, MEMS resonators offer a possibility for simultaneous filtering of the mixed signal due to the high mechanical quality factor and therefore a narrow passband of the resonators. This way a totally new component, mixer-filter or "mixler" [20] can be introduced. In addition to the new components enabled by the MEMS-technology even completely new radio-architectural approaches have been enabled. For example Otis et al. [32] present a RF-front end where the channel selection is performed with MEMS-resonators and A. T. Alastalo [25] suggests the use of micromechanical delay-lines in carrier regeneration. Another prominent architectural approach is presented in Chapter 3.4.

3.1 Background

We assume that a MEMS-resonator is excited with a signal at the frequency $f_{RF} = f_c + f_r$, where f_c is a carrier signal and f_r is the resonance frequency of a MEMS-resonator. The carrier frequency could typically be in the GHz-range and the mechanical resonance a few tens of MHz. In addition we assume that a local oscillator (LO) signal at the angular frequency $f_{LO} = f_c$ is present and that both the excitation and signal pick-up gap are DC-biased with the voltage U_{DC} (Fig. 17).

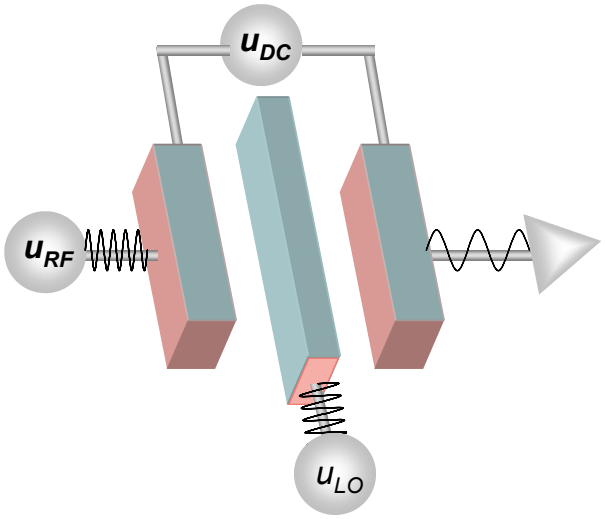

Fig. 17 Basic scheme of frequency mixing using micromechanical resonator.

The applied voltages can be written as:

Input (RF) signal: $u_{RF} = \hat{u}_{RF}(\sin \omega_{RF} t)$

Local oscillator (LO) signal: $u_{LO} = \hat{u}_{LO}(\sin \omega_{LO} t)$

Bias-voltage: U_{DC}

The total voltage at the transducer gap is $U = U_{DC} + u_{RF} + u_{LO}$. Due to the capacitive transduction Eq. (1.6), the force at the transducer becomes

$$F = \frac{1}{2}\frac{\partial C}{\partial x}(U_{Dc} + u_{RF} + u_{LO})^2 = \frac{1}{2}\frac{\partial C}{\partial x}(U_{Dc} + \hat{u}_{RF}(\sin \omega_{RF} t) + \hat{u}_{LO}(\sin \omega_{LO} t))^2 \tag{3.1}$$

Which can be written as

$$\begin{aligned} F = {} & \frac{1}{2}\frac{\partial C}{\partial x}(U_{DC} + 2\hat{u}_{RF} \sin \omega_{RF} t + 2\hat{u}_{LO} \sin \omega_{LO} t)U_{Dc} + \\ & + \frac{1}{4}\frac{\partial C}{\partial x}(\hat{u}_{RF}^2 + \hat{u}_{LO}^2 - \hat{u}_{RF}^2 \cos 2\omega_{RF} t - \hat{u}_{LO}^2 \cos 2\omega_{LO} t) + \\ & + \frac{1}{2}\frac{\partial C}{\partial x}[\hat{u}_{RF}\hat{u}_{LO} \cos(\omega_{RF} + \omega_{LO})t] + \\ & + \frac{1}{2}\frac{\partial C}{\partial x}[\hat{u}_{RF}\hat{u}_{LO} \cos(\omega_{RF} - \omega_{LO})t] \end{aligned} \tag{3.2}$$

It is evident, that the oscillation frequency of the last term of Eq. (3.2) is f_r. It is also clear that all the other frequency components are far away from the resonator passband and also filtered away as a consequence of the high quality factor of the MEMS-resonator. An important result is that the force is directly proportional to both input amplitudes $\hat{u}_{RF}$ and $\hat{u}_{LO}$. This conversion using LO-signal is depicted in frequency space in Fig. 18 a).

Eq. (3.2) is valid for capacitive devices. There are also other ways to realise frequency mixing. For example, devices exploiting thermal actuation have been presented in this context [85]. Effectively the thermal actuation also performs the quadratic mixing like the capacitive transduction but with a benefit of reportedly easier matching to the output of antenna or possible front-end electronics. Again this type of component is enabled by the MEMS-technology, since it is necessary to have micro sized or smaller devices to reduce the temperature response time to a feasible level ($\tau < 1$ µs). So far only interferometric measurements on such devices have been performed and therefore their true electrical operation has not been characterised fully. Also for the final realisation, the readout electronics will be capacitively coupled to the resonator and therefore the device will feature at least some of the drawbacks of the capacitive device.

Besides quadratic mixing of the signals due to the voltage-force nonlinearity also higher order mixing products can arise in capacitively coupled systems. The capacitive nonlinearity causes the cubic mixing of the input signals which generates the third order intermodulation (IM3) [86] that is responsible for converting out-of-band signals into in-band signals (Fig. 18 c and d). It has been shown [87,88] that the third order intermodulation distortion is mainly generated due to the capacitive non-linearity associated with the capacitive transduction and that there is a clear trade-off between the linearity and the motional resistance of a device. Despite this shortcoming, most of the reported micromechanical mixers have utilised the capacitive transduction both in frequency

conversion and down-converted signal pickup from the resonator due to the ease of realising the capacitive transduction.

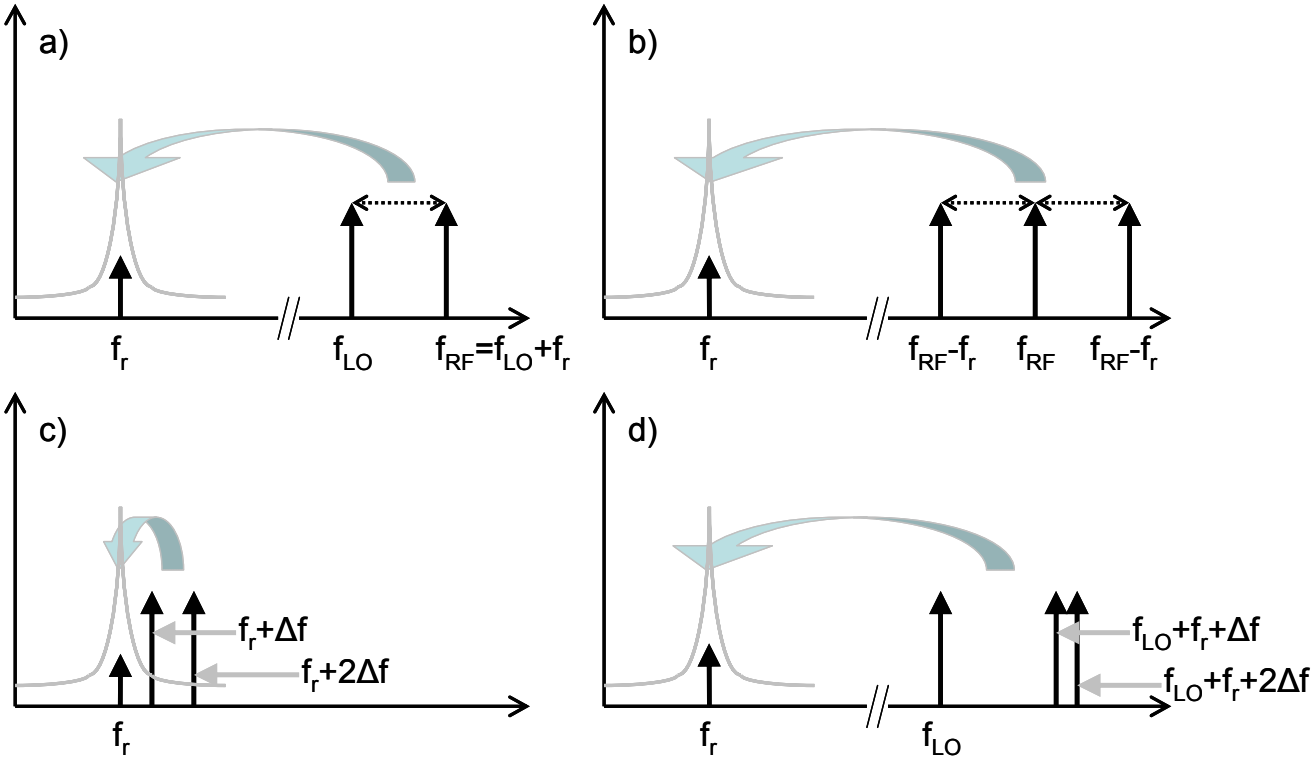

Fig. 18 Different conversion results from the non-linearities of MEMS. a) High-frequency signal converted with the aid of LO-signal b) AM-modulated high frequency signal converted intrinsically without LO-signal c) Third-order intermodulation (because of capacitive non-linearity) converts interfering signals outside the pass-band of a filter into the pass-band d) Similar to c), but with a high-frequency interferers converted with the aid of LO-signal and third-order capacitive non-linearity.

3.2 Micromechanical mixer-filter

Fig. 19 from [P3] shows a micromechanical resonator consisting of two mechanically coupled DETF-structures that is used as a mixer-filter. The device features a sub-µm coupling gap ($d \approx 170$ nm) which is used for highly efficient capacitive transduction in performing the frequency mixing. The mechanical coupling between the input and output is used to improve the isolation of the mixer due to the limited electrical conductivity of the coupling beam. At least two approaches can be taken when the device is used to convert a signal from high communication frequency down-to the resonance frequency of a MEMS-device: i) a local-oscillator (LO) signal is applied to the LO electrode to perform the conversion (Fig. 17 a) or ii) the input signal is selected so that the conversion takes place intrinsically without any LO-signal being applied (Fig. 17Fig. 18 b).

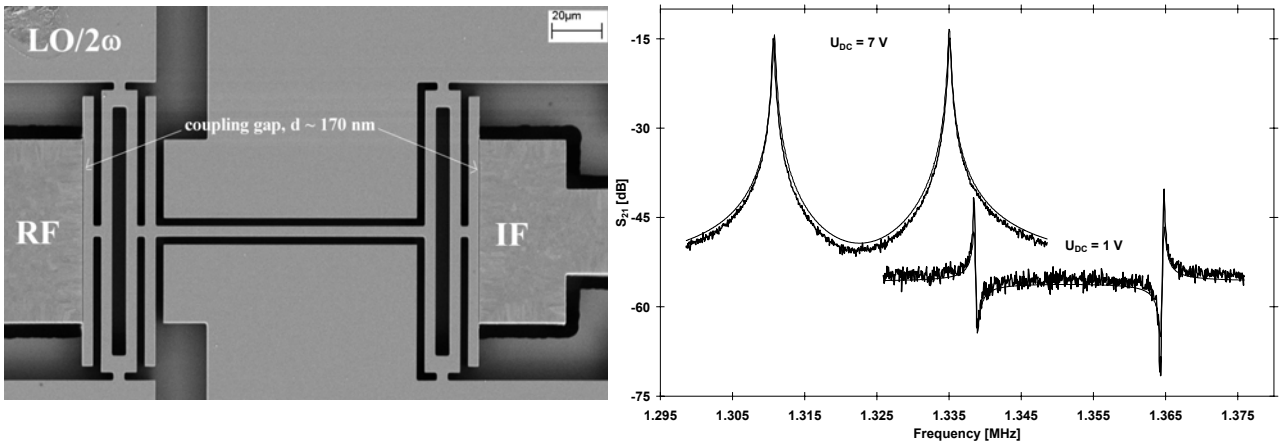

Fig. 19 a) Two mechanically coupled DETF-resonators used as a frequency mixer. b) Simulated and measured S_{21} responses of the system showing the first two resonances of the resonator. The effect of improved bias-voltage U_{DC} is illustrated clearly through improved coupling and increased capacitive-non linearity. Labels RF, IF and LO/2ω mark the corresponding electrodes used throughout the text.

3.2.1 Conversion with a local-oscillator

In [P7] the conversion performance of the presented device is characterised at three different LO-signal frequencies, $f_{LO} = [10, 100, 390]$ MHz with RF-signal at $f_{RF} = f_{LO} + f_{res}$ or $f_{RF} = [11.338, 101.338, 391.338]$ MHz, where f_{res} is the frequency of the first mechanical resonance of the device. The measured and simulated results with a LO-signal power $P_{LO} = 0$ dBm, RF-signal power $P_{RF} = -60$ dBm and bias voltage $U_{DC} = 7$ V are shown in Fig. 20.

The resonator was modelled as an electrical equivalent of the spring-mass system and for capacitive coupling an equivalent model taking into account the usual second order force-voltage Eq. (1.6) and also the third order capacitive non-linearity [89] was used. The model was generated with the transient simulations by modelling accurately the S_{21}- and phase-responses of the resonator with varying bias-voltages U_{DC}. The model was further refined by using a large-signal harmonic balance (HB) method utilising multiple independent input and output tones (excitation frequencies) and their harmonics to fit the model to the conversion measurements performed at carrier frequencies $f_c \gg f_{res}$. As the HB analysis is performed in frequency space it is a very efficient method when compared with the transient analysis in the case of devices with high quality factors and therefore long settling times [90].

It is evident From Fig. 20 that the device can be used to obtain nearly constant mixing performance up to $f_c = 400$ MHz which is mainly limited by the measurement instruments, not by the actual device. The high conversion loss includes the insertion loss and can be explained by the weak coupling of input-signals as the impedance of the resonator is much higher than 50 Ω. With proper impedance matching, which will become feasible when the coupling gap is fabricated so that $d < 100$ nm, the performance of the mixer will be improved. This is addressed in chapter 3.4.

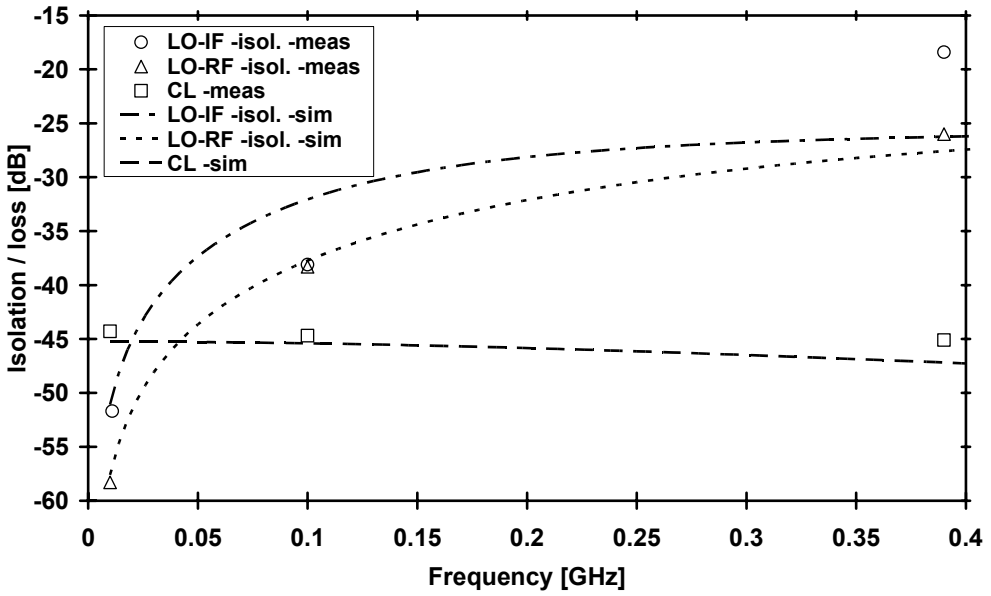

Fig. 20 Measured and simulated conversion loss (rectangles), LO-IF –isolation (circles) and LO-RF –isolation (triangles). The model gives excellent qualitative match even up to 400 MHz, except for the LO-IF –isolation where the model and the measurements agree quantitatively. The isolations were measured with a 50 Ω termination at the input and output of the device.

3.2.2 Conversion without local-oscillator

A new approach concerning the electrical excitation signal is needed if one wants to convert the excitation voltage down to a force at the resonance frequency of the device without any local oscillator. Instead of applying a signal with a single frequency component, a signal with multiple frequency components with a frequency separation equal to the resonance frequency of the resonator is used [P3,P7]. A good candidate for this approach is a high-frequency carrier signal that is amplitude-modulated (AM) at the resonance frequency of the device.

The input signal can be written as

$$\begin{aligned} U(t) &= \left[A_0 + B_0 \sin(2\pi f_m t)\right]\sin(2\pi f_c t) \\ &= A_0\left[\sin(2\pi f_c t) + \frac{h}{2}\sin(2\pi f_c \pm 2\pi f_m)t\right], \end{aligned} \tag{3.3}$$

where A_0 and B_0 are the amplitudes of the carrier and the modulation signal, respectively. The symbol f_c is the carrier frequency and f_m the modulation frequency, which in this case is also equal to the resonance frequency f_{res} of the resonator. The modulation index h is defined by $h = B_0/A_0$. The spectrum of the input signal can be seen from Fig. 18 b.

The down-conversion of the signal is done with the help of the non-linearity of the capacitive transduction Eq. (1.6). This non-linearity ensures that the arising force F has a component also at the resonance frequency $f_{res} = f_m$: (Derived in Appendix I)

$$F\big|_{\omega=\omega_m} = \frac{1}{2} A_0 B_0 \frac{\partial C}{\partial x}, \tag{3.4}$$

where $\partial C/\partial x$ is the electro-mechanical coupling factor. From Eq. (3.4) it is clear that is it convenient to have $A_0 = B_0$ or $h = 1$ as these factors play an equal role in contributing to the force.

In [P3] the idea of exciting the resonator using a GHz-range signal is studied. An AM-modulated GHz-range carrier signal is coupled to the resonator via the RF-electrode and the signal at frequency f_m is recorded from the IF-electrode with the aid of a DC-bias voltage $U_{DC} = 7$ V. The resonator is grounded via the LO-electrode.

Fig. 21 shows the measured and simulated output signal (V_{out}) of the resonator actuated with a modulated GHz-range signal (V_{in}, f_c = [0.5, 1.5] GHz). It indicates a successful excitation of a MHz-range resonator ($f_{res} = f_m = 1.338$ MHz) with a GHz-range signal without any LO-signal present at the resonator.

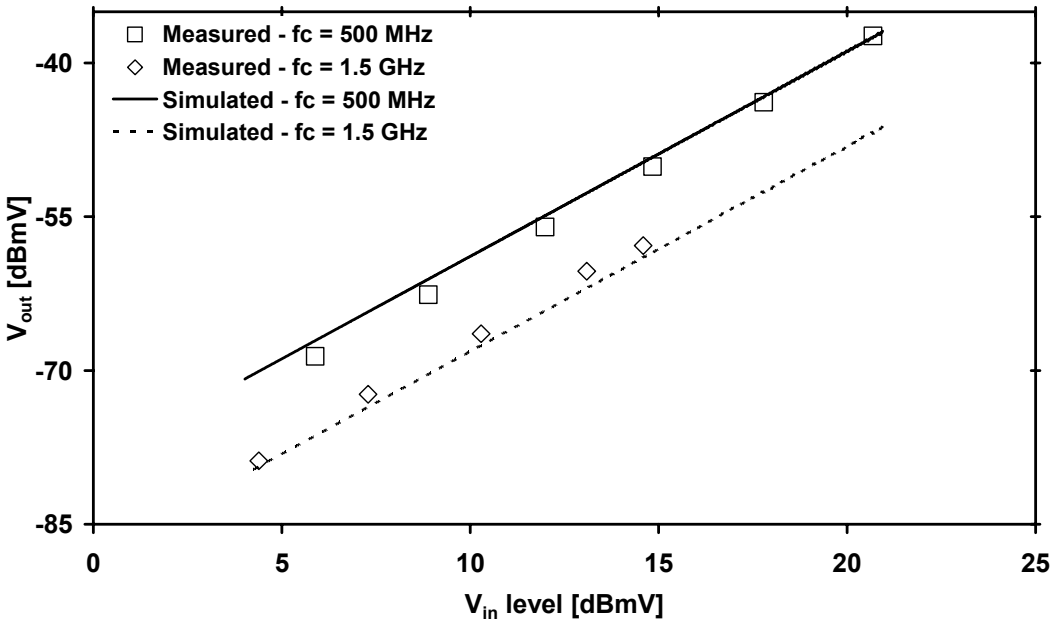

Fig. 21 Output signal voltage V_{out} as a function of input signal voltage V_{in}. The figure indicates a successful excitation of a MHz-range resonator with GHz-range signal as the carrier frequency of the excitation signal is f_{in} = [0.5, 1.5] GHz and the recorded output signal frequency is $f_{out} = f_m = 1.335$ MHz.

As Fig. 21 demonstrates the conversion loss increases if the carrier frequency is even further increased. Based on simulations, the rate of the decrease is found to be approximately 8 dB per GHz [P3]. The decrease in the performance can mainly be attributed to the parasitic capacitances of the system.

The weakness of the output signal can again be partially explained by very weak coupling of the input signal as was also the case in Chapter 3.2.1. An additional explanation comes from Eq. (3.4) as the force at the resonance frequency is the product of two fairly small ac-signals, the strong LO-signal being absent. Again, by reducing the coupling gap d and with impedance matching the performance can be increased.

Table V lists some results of performance of micromechanical mixers. Note that both the conversion loss and isolations are given at the maximum f_{RF} (and therefore maximum f_{LO}) frequency.

Table V – Conversion, isolation and frequency properties of various published micromechanical mixers.

Device	CL [dB]	P_{LO} [dBm]	f_{IF} [MHz]	$I_{LO\text{-}IF}$ / $I_{LO\text{-}RF}$ [dB]	f_{RF} converted [MHz]	Comment
DETF [22]	48	0	0.743	36 / 48	10	
Coupled DETF [22]	54	0	0.660	56 / 68	10	
Cantilever [21]	39	13	0.435	Not reported	400	Upto 3.2 GHz converted, but not reported
C-c[1] beam [23]	75	5	22.5	58 / 82	1000	
C-c[1] beam [91]	125	10	220	97 / 89	232	
Coupled c-c[1] beams [20]	13	15	37	39 / 29	242	
Coupled ring-resonators [92]	83.5	27	423	Not reported	438	2-mode mixer used to achieve 0.05% ripple
Coupled DETF [P7]	44 45	0	1.3	26 / 18	100 400	Sub-μm coupling gap
Coupled DETF – AM [P3]	62[4] 70[4]	N/A[2]	1.3	N/A[2]	500 1500	Sub-μm coupling gap
Coupled DETF[3] [P7]	8	0	1.3	29 / 35	100	Simulated improvements
Coupled DETF[3] – AM [P3]	15[4]	N/A[2]	1.3	N/A[2]	500	Simulated improvements
ADEX-10L	8	4	800	21 / 48	1500	Surface mountable diode-ring mixer

[1] Clamped-clamped beam.

2 Input signal is AM-modulated, no local oscillator is used.

[3] Coupling and efficiency improved in circuit simulator

[4] For an AM-modulated signal downconversion, the conversion loss is proportional to the input signal power (3.4) due to the multiplication of the spectral components. Value presented here is then the power of all the spectral components is P_{in} = -30 dBm.

The conversion losses reported in Table V are plotted on Fig. 22. For justified comparison the conversion losses are normalised to a local oscillator power P_{LO} = 0 dBm by Eq. (3.2).

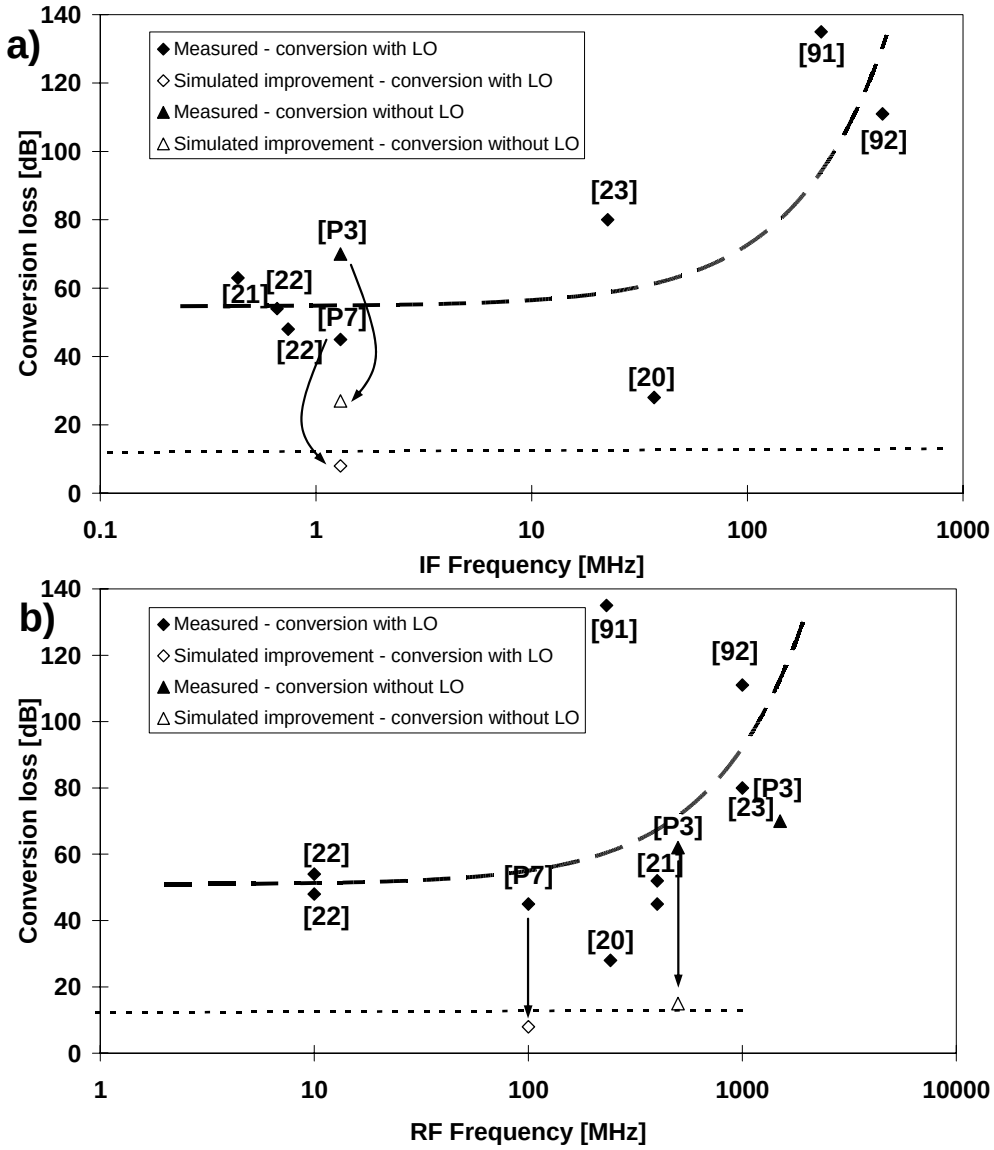

Fig. 22 Conversion losses of some published micromechanical mixer-filters as a function of a) IF- and b) RF-frequency. The dashed line is a linear fit to the data (conversion with LO) to emphasise the degradation of the performance with increased frequency. Dotted line represents a conversion performance of a commercial surface mountable mixer (ADEX-10L) given as a reference. The arrows indicate the possible improvements that have been simulated in Chapters 3.3 and 3.4.

From Table V and Fig. 22 it can be seen that the conversion losses for MEMS-based mixers are large when compared with for example a diode-ring mixer. Due to that the rest of the Chapter is dedicated to improving the conversion performance and to bringing the conversion loss to a usable level. This would allow taking the advantage of the added benefit of combined filtering with mixing fully and it is shown through the simulated results in [P3] and [P7] that MEMS mixlers can offer comparable or even better conversion performance as macroscopic diode-ring mixers.

3.3 Parametric amplification of mixer-filter

Besides increasing the LO-power or the coupling of the input signals, another approach to improve the downconversion of the signals is the use of mechanical parametric amplification. Previously for

micromechanical systems, parametric amplification has been utilized to tune the performance of mechanical resonators and oscillators [22,93-96], various sensors [97-99] and even filters [100]. In parametric amplification, one well defined physical quantity that is essentially affecting the resonance is modulated at a frequency $2\omega_0/n$, where n is an integer. Usually for micromechanical devices this physical property that is modulated is the mechanical spring constant. Normally this is done by changing the electrical spring constant, k_e, Eq. (1.12) through the gradient of the electric field, but also other schemes like spring constant modulation through the change of mechanical stress due to optical heating with laser [95] have been proposed.

The equation of motion in case of parametric amplification by the modulation of the spring constant is

$$m\ddot{x} + \frac{m\omega_0}{Q}\dot{x} + \left[k_0 + \Delta k \sin(2\omega_0 t)\right]x = F_0 \cos(\omega_0 + \varphi), \tag{3.5}$$

where Δk is the modulation amplitude of the spring constant and φ is the phase difference between the exciting and the pumping signals.

The solution for Eq. (3.5) is [93]

$$x(t) = \frac{F_0 Q}{k_0}\left(\frac{\cos\varphi}{1+\frac{Q\Delta k}{2k_0}}\sin(\omega_0 t) + j\frac{\sin\varphi}{1-\frac{Q\Delta k}{2k_0}}\cos(\omega_0 t)\right), \tag{3.6}$$

from which the parametric gain can be calculated to be

$$G = \left[\left(\frac{\cos\varphi}{1+\frac{Q\Delta k}{2k_0}}\right)^2 + \left(\frac{\sin\varphi}{1-\frac{Q\Delta k}{2k_0}}\right)^2\right]^{1/2}. \tag{3.7}$$

From Eq. (3.7) one can deduce that the amplification is phase-sensitive and reaches its maximum when the phase-difference is $\varphi = \pi/2$ between the exciting and pumping signals. Another point worth noting from Eq. (3.7) is that the modulation of the spring constant results in a spontaneous oscillation of the system when $Q \times \Delta k/k_0 = 2$ despite the input signal being absent. Therefore for the actual realization, both the amplitude and the phase of the pumping signal must be accurately controlled.

The particular mixer-filter shown in Fig. 19 (page 32)device is ideal for parametric amplification as the narrow coupling gap combined with rather low k_0 allows a large modulation of the spring constant with a moderate pumping voltage Eq. (1.12). In [P6] the parametrically amplified downconversion of an AM-modulated RF-signal is performed with a setup that is identical to that presented in Chapter 3.2.2 with an additional pump signal at the 2ω-electrode. The results for the amplification for various pump-powers can be seen in Fig. 23 [P6]. An improvement in the excess of $G = 30$ dB can be reached, but the system is very close to spontaneous oscillations as $Q \times \Delta k/k_0 \approx 2$ at these gain levels (Fig. 23 a).

An interesting novel observation is related to the required pump powers. As Fig. 23 demonstrates, an appropriate pump power depends on the particular resonance mode in question. The explanation can be found from Fig. 19 as the excitation and read-out electrodes lie on the opposite sides of the resonator but the pump signal is coupled to the resonator itself. Therefore the pump-signal leads to the modulation of the spring constant of the outermost beams only, but due to the fact that there are no electrodes next to the interior beams, the gradient of the electric field is very low leading to almost negligible modulation of the spring constant.

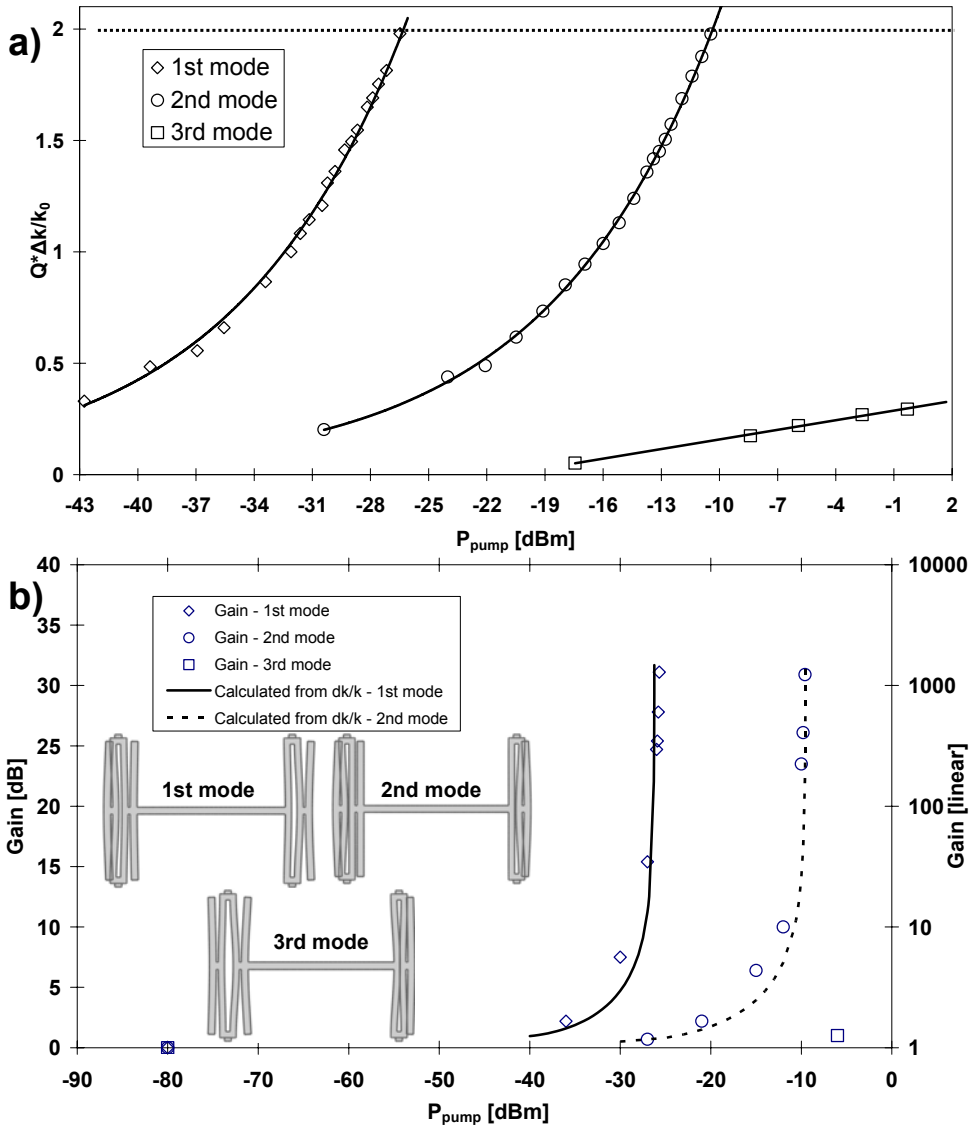

Fig. 23 a) Modulation of the spring constant $\Delta k/k_0$ when the pump signal is applied to the 2ω electrode. Dotted line marks the limit of spontaneous oscillation. b) Gain as a function of pump (2ω) power for the first three eigenmodes (shown as insets) shows the power needed for amplification in each case. The measured limits for spontaneous oscillation are -25.6 dBm and -9.3 dBm for first and second mode, respectively. Solid and dashed lines represent the gains calculated (Eq. (3.7)) from the measured values of modulating the spring constant shown in a).

From Eq. (3.2) we see that increasing the LO- or input RF-power increases directly the conversion efficiency of a mixler. Also from Eq. (3.4) is can be seen, that when using an AM-modulated signal, the conversion efficiency is increased to the second power of the input RF-power if the spectral components of the input signal are similar. However, from Fig. 23 b) it is evident, that when using

the parametric amplification, the increase can be an exponential function of the pump power. Therefore for low-power applications, the mechanical frequency mixing that is further improved by parametric amplification enabled by MEMS seems to be a tempting approach.

3.4 Radio-architectural concepts

New radio-architectures can be enabled by the MEMS-technology presented in this thesis. A MEMS-mixler can be used as a part of a receiver. For this, a protocol where the information is modulated in relative amplitudes or phase differences of two or more carriers can be used. The information is then "revealed" using the capacitive transduction and the resonances of MEMS-resonators. In even simpler approach, if only one eigenfrequency of the MEMS-device is used, this can be used to establish an on-off –keying (OOK) modulation where the status of a bit is defined by a carrier frequency being present or absent. By parallelising these kinds of resonators or choosing a multi-resonant (like DEFT or 2D BAW) device a slightly more efficient frequency-shift- keying (FSK) modulation can be performed.

A multi-resonant resonator can be utilized as a receiver in a system, where the data is modulated using for example relative amplitudes of multiple carrier frequencies like in OFDM system (Orthogonal Frequency Division Multiplexing). As an example of such a system [P3] demonstrates an FSK-reception where the information is coded into the two eigenfrequencies of mechanically coupled DETF-structures. One example to test such an approach is shown in Fig. 24. The input signal is selected so that the sidebands closer to the carrier are separated from the f_c = 1.5 GHz carrier by f_{r1} = 1.308 MHz and the sidebands that are even further away in frequency by f_{r2} = 1.335 MHz. The separations coincide with the first and the second eigenfrequency of the resonator, respectively. In this measurement the amplitudes of the sideband components differ by 8.5 dB. Fig. 24 c) shows the output signal picked from the DC-biased IF-electrode. It clearly shows that the same relative amplitude difference of the input signal is maintained through the downconversion of the signal. This indicates that the principal idea of utilising multiresonant micromechanical resonator as an FSK-receiver is valid.

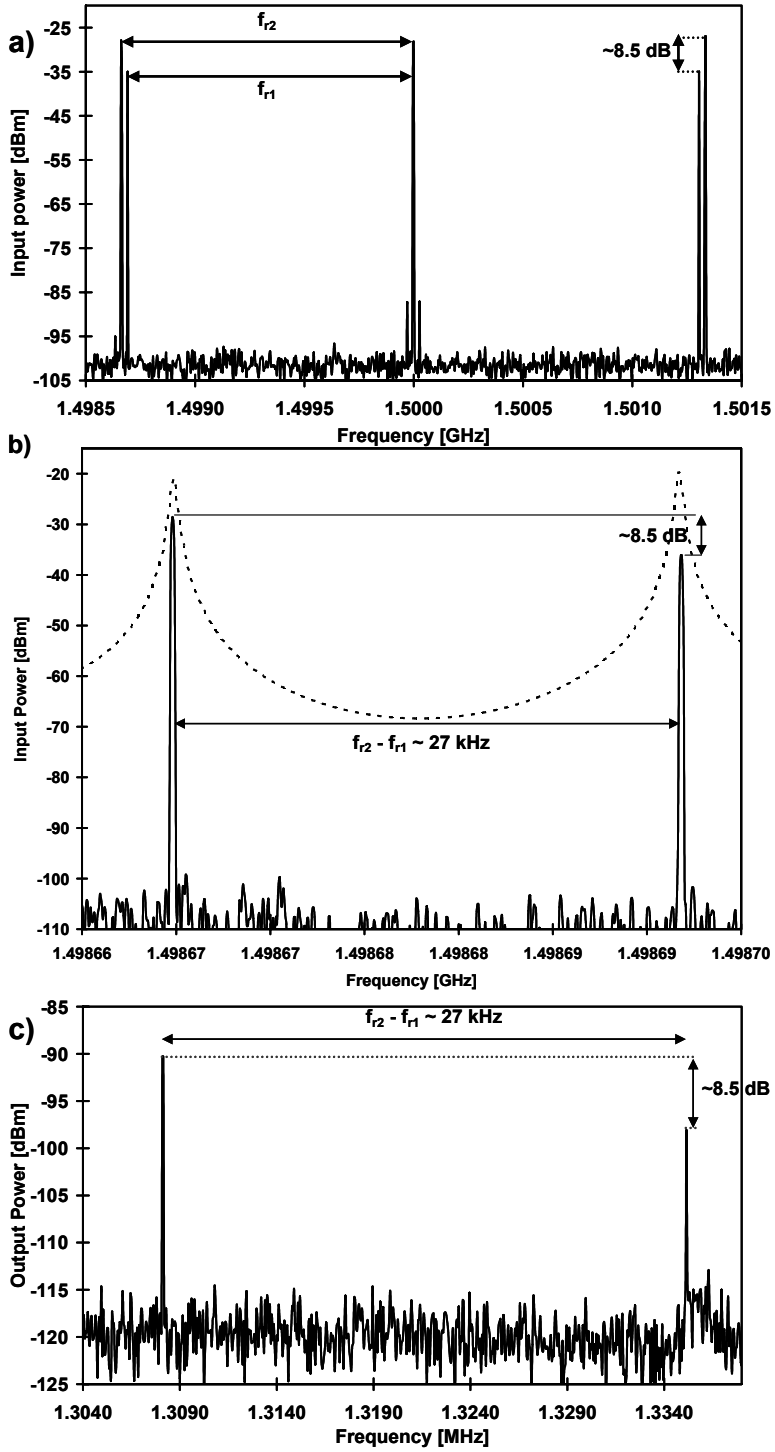

Fig. 24 The spectrum of the input signal in the FSK reception measurement. a) The carrier frequency is f_c = 1.5 GHz of which the sidebands are separated by f_{r1} = ±1.308 MHz and f_{r2} = ±1.335 MHz. b) Detailed view of the two lower sidebands. The dashed line represents the transfer function of the resonator used as a mixler. c) The measured signal from the IF-electrode of the resonator indicates that the relative amplitude difference of the input signal at GHz is maintained through the downconversion of the signal. All the cases represent a situation when bit 0 is transmitted. Note the change of the order of magnitude in the x-axis in c).

From Fig. 24 one can observe that for practical application the proposed method exhibits quite a large conversion loss. One way to improve the conversion performance would be to utilize the parametric amplification as presented in Chapter 3.3. Another way would be to improve the

coupling and by that enable the better matching between the MEMS and the input-system. In addition, the high-frequency performance of the system will be improved by reducing the parasitic capacitances that are caused by the bonding pads. These pads are needed for the characterisation of the device, but for actual integrated device they could be fabricated significantly smaller.

The previously mentioned improvements in the conversion performance of a mixler were studied in [P7]. This was done with the help of a circuit simulator [101] that is capable of simulating MEMS-devices through their electrical equivalents. Before studying the improvements an accurate model of the mechanical resonator and the measurement circuit was generated. The model was based both on low and high frequency measurements taking into account both linear and higher order effects up to the third order. After that the model was modified by first reducing the coupling gaps to $d = 100$ nm while maintaining the bias-voltage at $U_{DC} = 7$ V, which is very close to the pull-in voltage of the device $U_{pi} = 7.5$ V. Keeping the other parameters intact, this reduces the mechanical impedance of the system from $R_m = 15$ kΩ to $R_m = 1.7$ kΩ. Then an impedance matching circuit was used to match the input for the MEMS and the bonding pad capacitances were lowered from $C_{pad} = 4.9$ pF to $C_{pad} = 49$ fF. The results compared with Fig. 20 can be seen from Table VI.

Table VI - Improvements gained with the impedance matching and parasitic capacitance reduction.

		Measured device	Improved device
d	[nm]	170	100
U_{DC}	[V]	7	7
Impedance match		No	Yes
C_{pad}	[pF]	4.9	0.049
f_{IF}	[MHz]	100	100
CL	[dB]	44	**8**
LO-IF isol.	[dB]	30	29
LO-RF isol.	[dB]	38	35

Similar improvements have also been reported for AM-modulated signal downconversion [P3].

4 Fabrication process for fast prototyping of MEMS-devices for research purposes

Up to a certain point, simulations and mathematical models can be used to predict the performance of MEMS-devices. However, to really study the applicability of MEMS-devices for various applications a process to fabricate actual devices is needed. MEMS fabrication processes are usually based on the knowledge gained in the integrated circuit (IC) fabrication. Therefore a typical MEMS fabrication process consists of subsequent steps of lithography, deposition and etching. In addition to these, the first step in manufacturing is usually the design and fabrication of the photomasks that are needed during the different process steps.

Usually the (photo) mask fabrication takes time. This is especially true in the research laboratories as the mask fabrication is usually done as an external service. Of course once the mask is fabricated it can be used to produce identical devices over and over again, but for research purposes this gives no flexibility as each time a new concept is generated a new mask has to be fabricated.

Instead of using a physical hard mask and conventional optical lithography, direct writing of the mask using electron beam (E-beam) lithography is a viable option. In this approach the desired features are directly patterned on the substrate by exposing an electron sensitive photoresist (e.g. PMMA) with an electron beam. The beam is generated by a scanning electron microscope (SEM) with special software. As a drawback the exposure area is usually limited (for example to 1×1 mm^2) when compared with a full wafer that can be exposed by optical lithography. Also the exposure speed is low (for example $t = 3$ h to expose 1×1 mm^2). Due to these limitations E-beam exposure is a valid approach when fabricating a small number of devices, for example in prototyping. The main benefit comes from the fact that once the desired features are designed on a computer, they can be immediately patterned on a substrate and devices can be fabricated without the need of a separate time consuming mask fabrication step. Also the resolution of the E-beam lithography is superior to conventional optical lithography by mask aligners.

[P4] presents a fabrication process that takes advantage of E-beam lithography in the fabrication of MEMS-devices. The process was developed with two goals in mind: i) Short time from mask design to finalised device and ii) Good electromechanical coupling, that is ensured by small enough features.

The first goal was addressed with the use of E-beam lithography as suggested previously. In addition, the release etching was performed with Cryogenic Inductively Coupled Plasma Deep Reactive Ion Etching (Cryo-ICP DRIE) instead of typically used HF(-acid) followed with supercritical CO_2 drying. In the presented approach the problem of device stiction due to the capillary forces is overcome without separate drying of the etchant. Usually DRIE is used for anisotropic etching to define the vertical trenches. However, when the anisotropic etching reaches the buried oxide (BOX) of a Silicon on Insulator (SOI) -wafer, the etching commences isotropically at the silicon – BOX interface [102]. Fig. 25 a) shows an example of this *notching* phenomenon. Similar “dry-processes” have been used in the fabrication of accelerometers [103], switching devices [104] and resonators with eigenfrequencies in the kHz range [105,106]. All of these have used the Bosch process DRIE [107], however.

The use of dry-etching also for the release increases the total dry-etching etch time. This in turn requires increased endurance of the etching mask which is usually solved by increasing the mask

thickness. This in turn degrades the resolution of the process. In [P4] Atomic Layer Deposited (ALD) Al_2O_3 (alumina) is used as an etching mask material to overcome the need for thick mask as it has been shown to feature extremely high selectivity to silicon in cryogenic etching (even 1:70 000) [108]. Due to this only a few nm thick layers of Al_2O_3 were used in the fabrication (Fig. 25 b). This makes the step of etching the openings to the alumina non-critical. In addition to the use of alumina as etching mask material, the improved resolution of the E-beam lithography serves the goal of improving the electromechanical coupling. The process combining the aforementioned features is depicted in Fig. 26.

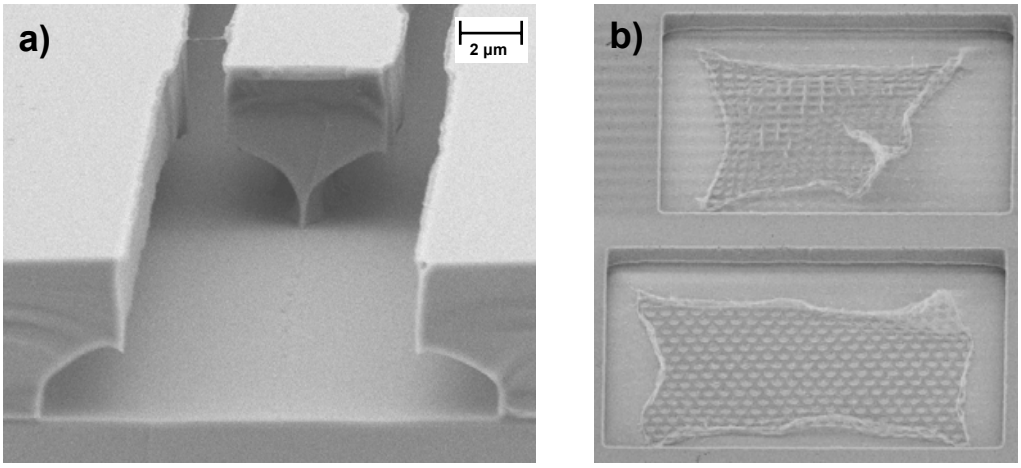

Fig. 25 a) A micromechanical beam resonator before release with the help pf the notching effect. The vertical trenches have been etched with anisotropic cryogenic DRIE to define the capacitive coupling gaps. Once the anisotropic etching reaches the buried oxide, the etching commences isotropically at the interface eventually performing the release of the device. b) A few nm thick Al_2O_3 film that is used as an etching mask is revealed after etching away a large area of silicon underneath the film. The films are curled, but otherwise they look intact.

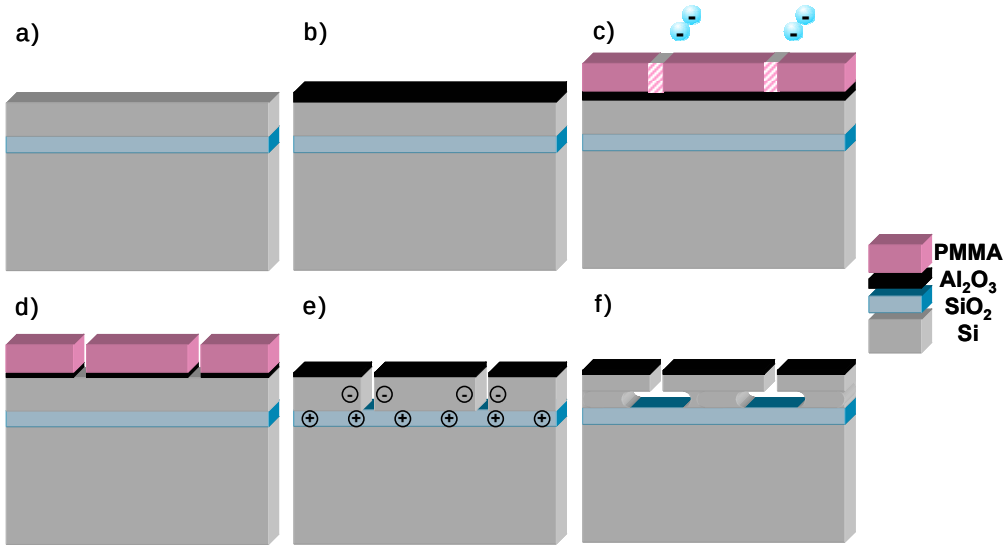

Fig. 26 Fabrication process (not to scale): a) SOI-wafer b) Al_2O_3 film is deposited using atomic layer deposition (ALD) c) PMMA is spun on alumina and exposed by e-beam d) PMMA is developed and alumina is etched by reactive ion etching (RIE) to form a hard-mask for silicon etching. Afterwards PMMA is removed in oxygen plasma. e) Silicon is etched in cryo DRIE with alumina as hard mask to define the structures g) When the etching reaches the buried oxide is continued after reaching the buried oxide, notching releases the device. It is evident from the figure that widths of the openings in the alumina in step d) are very tolerant to over-etching.

The process parameters are characterised with test structures that are used to determine the amount of underetch (notching) and the final width of the coupling gap to see the limiting factors in the process and possible optimisation paths. As a test ten trenches with variable widths were etched with the process and the cleaved cross-section was carefully analysed with SEM – this was done for a number of different etching times and temperatures. As the cryo-ICP process gives a possibility of cooling the samples during etching, different etching-cooling cycles were also tested. The results of one such a test in Fig. 27 shows that features with width up to $w = 5$ µm can be realised while still maintaining the coupling gap below $d < 1.5$ µm. Also the limiting factors for the release can be seen. For wide gaps, the notching effect weakens and vanishes when $h/d \approx 1$. [P4] shows that in this parameter region the notching cannot be increased by increasing the etching time. However, for higher *h/d* ratios (i.e. for lower *d*), the limiting factor is the *RIE-lag* which causes the features with higher *h/d* ratio to etch slower [109]. Therefore for the features with higher *h/d* ratio in the left side of the figure the notching can be improved with increased etching time.

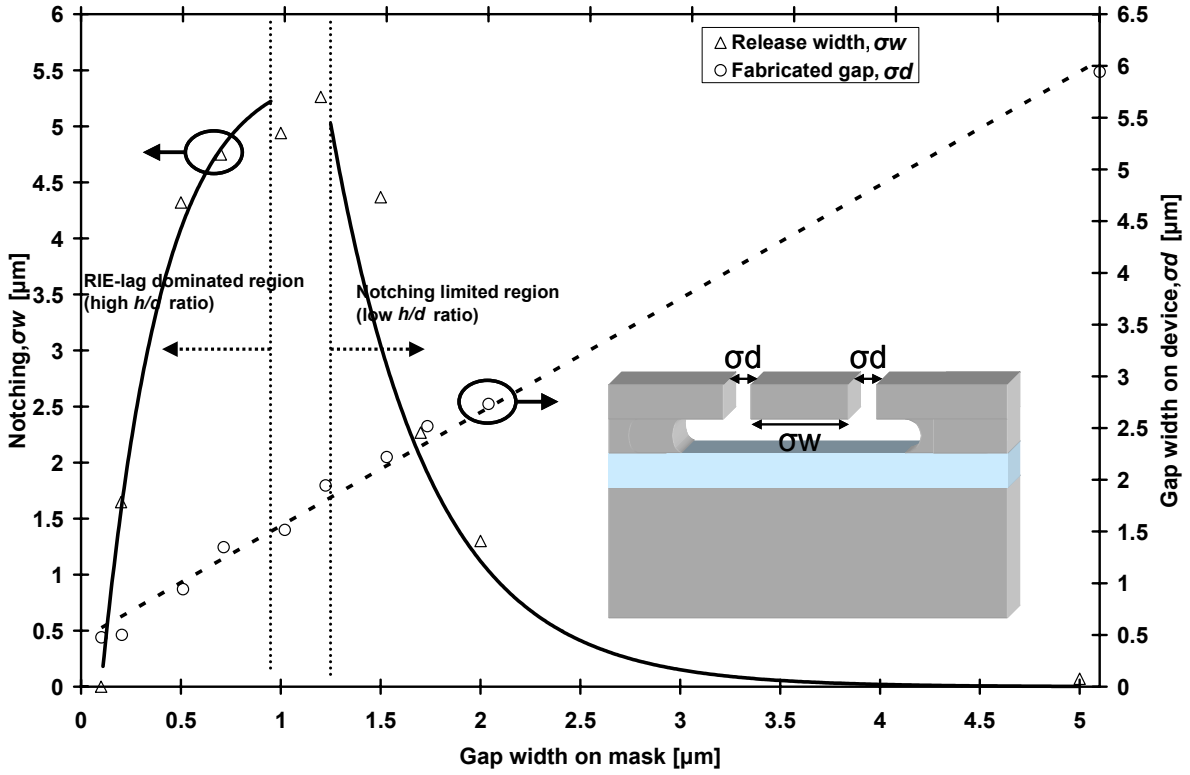

Fig. 27 The horizontal-axis shows the designed gap width on the mask. Circles (o) and dotted line indicate the actual fabricated coupling gap. The width of the released area is shown in triangles (Δ) with solid lines as exponential fits to the measured data. The release width for narrow gaps ($d < 1$ µm, i.e. high *h/d* ratio) can be increased by increasing the etching time as the limiting factor is the RIE-lag. The thickness of the device layer is $h = 4$ µm. From this figure straightforward design rules can be extracted.

In addition to test structures several resonators have been fabricated with the process. Fig. 28 a) and b) show a fabricated DETF-resonator and a S_{21} response of the device, respectively. Fig. 28 b) reveals that the quality factor of the resonator ($Q \approx 8\,000$) is comparable with the devices fabricated with conventional SOI-microfabrication methods [22,110].

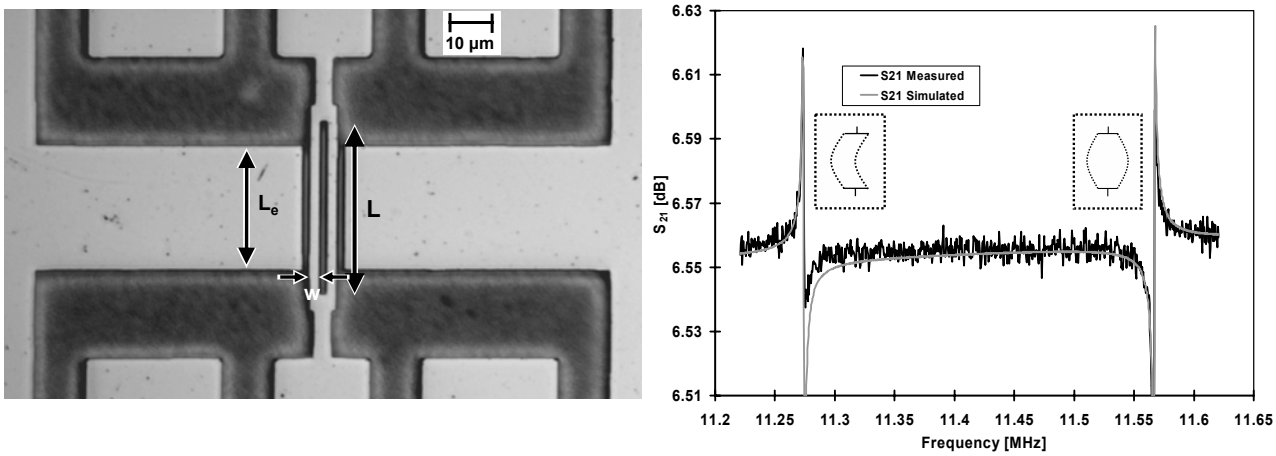

Fig. 28 An optical image of a fabricated tuning fork resonator. The letters *L* and *w* denote the length and the width of the resonating beams, respectively. L_e is the length of the electrode. Measured and simulated S_{21} responses of a fabricated resonator r reveal that the resonator is released and working. The two vibrational modes of the resonator indicate modes where the beams move either in-phase or in anti-phase.

5 Summary

This Thesis presents the studies on the microelectromechanical devices for RF-applications done by the author during the period 2002 – 2007. The focus of the work has been in the frequency reference and frequency conversion applications and the aim has been to study the relevant parameters concerning the stability and performance of microelectomechanical resonators in the aforementioned applications. In addition to own work the work of the groups working in the field has been reviewed.

The Thesis shows that using micromechanical resonators as a replacement for macroscopic quartz-crystal it seems possible to realise a high precision frequency reference. Relevant parameters concerning short- and long-term stability were reviewed and it was shown that an oscillator with a phase-noise $\mathscr{L}_f$ = -138 dBc/Hz at Δf = 1 kHz offset from the f_c = 13 MHz carrier and with a noise-floor of $\mathscr{L}$ = -150 dBc/Hz can be realised. It was also shown that to reach a long-term stability required by any practical frequency reference application the resonator must be protected from the ambient atmosphere. However, it was shown that the protected bulk acoustic mode resonators show a frequency stability better than $df/f < \pm 1$ ppm during the measurement time of t = 1000 h and based on the linear extrapolation of the measured data the resonators show a frequency drift that suggests a capability to keep the centre frequency requirement of even a GSM reference oscillator for a period exceeding one year.

Currently micromechanical silicon resonators are being applied in oscillators applicable for clock generation for various consumer and industrial markets. The results presented in the Thesis show that silicon micromechanical resonators offer a competitive alternative for quartz crystals also in the realisation of high precision frequency references. However, the studies on the stability were performed by removing the effect of the temperature by mathematical means and therefore the issue of practical temperature compensation of the output frequency remains to be answered. An accurate method to measure the temperature of the silicon resonator has been demonstrated and also compensation schemes based on the accurate measurement of the temperature have been suggested.

The drift rate of the micromechanical resonators was based on the linear extrapolation of the measurement data and as the extrapolation to longer times should always be taken with care, it is important to verify the drift in a longer period.

As a related stability issue, a method to measure the built-in potential of capacitive micromechanical devices was presented. The built-in potential has been seen to be a factor contributing to the stability degradation in MEMS voltage-references and various micromechanical capacitive sensors. The demonstrated method is based on the vibrating capacitor (Kelvin probe) principle and it was demonstrated by measuring the built-in potential of capacitive accelerometers with a good accuracy when compared with existing capacitance-voltage measurement.

As another application area the potential of frequency conversion using micromechanical resonators as mixers was addressed. The performance of the devices to convert gigahertz-range communication frequency down to the eigenfrequencies of the resonators (megahertz-range) was studied by using the voltage-force non-linearity of the micromechanical coupling gap as the non-linearity that is used to perform the multiplication of the input signals. Among all the non-linearities present in micromechanical resonator, the one selected is common to all devices exhibiting capacitive transduction and is usually the strongest one. In the Thesis the conversion was performed successfully using various high frequency carriers up to f_c = 1.5 GHz, which was limited by the

measurement setup. In addition to traditional conversion with a local oscillator signal a method for intrinsic conversion using AM-modulated signal was demonstrated. In the second approach the amplitude of the input signal is modulated at the resonance frequency of the mixing resonator and the capacitive transduction ensures the force at the frequency of modulation that is also the resonance frequency of the mixer. However it was noted that for both conversion methods, the performance of the mixler was rather poor exhibiting the conversion loss in the range of CL ≈ 50 dB. The poor conversion performance was noted to be a problem with all published micromechanical mixers and it was credited to the high mechanical impedance and large bonding pad capacitances of the mixer. An accurate model of the micromechanical mixer was generated based on the various low- and high frequency measurements and it was shown that performance improvements in the order of almost 50 dB are achievable by improving the impedance match between the mixer and input electronics after lowering the mechanical impedance of the resonator and reducing the bonding pad capacitances.

Parametric amplification was suggested as an active method to improve the conversion performance and demonstrated it was demonstrated to bring a performance improvement of over 30 dB. As an example of new approach in new architectural approaches, a method for coding the information bits and demodulating the information with multiresonant micromechanical resonator in a MEMS radio receiver was demonstrated.

Finally a process for fast prototype fabrication of micromechanical devices was presented and tested by fabricating micromechanical DETF resonators that exhibit quality that is comparable with similar resonators fabricated with conventional SOI micromachining. The process was demonstrated on $h = 4$ μm thick SOI-wafer by fabricating micromechanical resonators with the proposed fabrication process, but in order to fabricate competitive devices in terms of electromechanical coupling the process has to be upgraded to $h = 10$ μm thick wafer. However, by careful characterisation of the limiting factors of the process it became evident that improving the h/d ratio should be no problem, but could be realised with increased etching time. This should be feasible due to the extremely durable atomic layer deposited Al_2O_3 film that is used as an etching mask.

References

[1] K. E. Petersen, "Silicon as a mechanical material", *Proc. IEEE*, **70**, pp. 420-457 (1982).

[2] G. M. Rebeiz, *RF-MEMS, Theory, Design and Technology*, John Wiley & Sons inc. (2003).

[3] I.-J. Cho, T. Song, S.-H. Baek, and E. Yoon, "A low-voltage and low-power RF MEMS series and shunt switches actuated by combination of electromagnetic and electrostatic forces", *IEEE Transactions on Microwave Theory and Techniques,* **53**, pp. 2450-2457 (2005).

[4] Q. X. Zhang, A. B. Yu, L. H. Guo, R. Kumar, K. W. Teoh, A. Q. Liu, G. Q. Lo and D.-L. Kwong, "RF MEMS switch integrated on printed circuit board with metallic membrane first sequence and transferring", *IEEE Electron Device Letters,* **27**, pp: 552–554 (2006).

[5] M. Daneshmand and R. R. Mansour, "C-type and R-type RF MEMS Switches for Redundancy Switch Matrix Applications", *IEEE MTT-S International Microwave Symposium Digest*, pp. 144-147 (2006).

[6] Teravicta inc. [Online] Available: www.teravicta.com.

[7] Magfusion inc. [Online] Available: www.magfusion.com.

[8] R. Aigner, "MEMS in RF-filter applications: thin film bulk-acoustic-wave technology", in *13th International Conference on Solid-State Sensors, Actuators and Microsystems (Transducers '05)*, pp. 5-8 (2005).

[9] B. Pillans, S. Eshelman, A. Malczewski, J. Ehmke, and C. Goldsmith, "Ka -band RF MEMS phase shifters", *IEEE Microwave and Guided Wave Letters*, **9**, pp. 520-522 (1999).

[10] N. Kingsley, D. E. Anagnostou, M. M. Tentzeris and J. Papapolymerou, "RF MEMS sequentially reconfigurable Sierpinski antenna on a flexible organic substrate with novel DC-biasing technique", *J. Microelectromech. Syst.*, **16**, pp. 1185-1192 (2007).

[11] C. won Jung, M.-J. Lee, G. P. Li, and F. De Flaviis, "Reconfigurable scan-beam single-arm spiral antenna integrated with RF-MEMS switches*", IEEE Trans. Antennas and Propagation*, **54**, pp. 455-463 (2006).

[12] W. Guoan, T. Polley, A. Hunt, and J. Papapolymerou, "A high performance tunable RF MEMS switch using barium strontium titanate (BST) dielectrics for reconfigurable antennas and phased arrays", *Antennas and Wireless Propagation Letters*, **4**, pp. 217-220 (2005).

[13] A. Dec and K. Suyama, "Microwave MEMS-based voltage-controlled oscillators", *IEEE Transact. Microwave Theory Tech.*, **48**, pp. 1943-1949 (2000).

[14] A. Coustou, D. Dubuc, K. Grenier, E. Fourn, O. Llopis and R. Plana, "Capabilities of a 10 GHz MEMS based VCO"; in*. 1st European Microwave Integrated Circuits Conference*, pp. 157-160 (2006).

[15] V. K. Saraf, D. Ramachandran, A. Oz, G. K. Fedder, and T. Mukherjee, "Low-power LC-VCO using integrated MEMS passives", in *IEEE Radio Frequency Integrated Circuits Symposium 2004 (RFIC 2004)*, pp. 579-582 (2004).

[16] L. Lin, C. T.-C. Nguyen, R. T. Howe and A. P. Pisano, "Microelectromechanical filters for signal processing", in *IEEE International Conference on Micro Electro Mechanical Systems (MEMS'92)*, pp. 226-231 (1992).

[17] L.Lin, R. T. Howe and A. P. Pisano, "Microelectromechanical filters for signal processing", *J. Microelectromech. Syst.,* **7**, pp. 286-294 (1998).

[18] SiTime inc. Available [Online]: www.sitime.com.

[19] Discera inc. Available [Online]: www.discera.com.

[20] W. Arc-Chew and C. T-C. Nguyen, "Micromechanical mixer-filters ("mixlers")", *J. Microelectromech. Syst.*, **13** pp. 100-112 (2004).

[21] F. Chen, J. Brotz, U. Arslan, C-C. Lo, T. Mukherjee and G.K. Fedder, "CMOS-MEMS resonant RF mixer-filters", in *18th IEEE International Conference on Micro Electro Mechanical Systems (MEMS 2005)*, pp. 24-27 (2005).

[22] A. T. Alastalo, M. Koskenvuori, J. Kiihamäki and H. Seppä, "A micromechanical resonating RF mixer", in *34th European Microwave Conference (EuMW2004),* pp. 1297-1300 (2004).

[23] A. Uranga, J. Verd, J. L. Lopez, J. Teva, G. Abadal, F. Torres, J. Esteve, F. Perez-Murano and N. Barniol, "Fully integrated MIXLER based on VHF CMOS-MEMS clamped-clamped beam resonator", *Electron. Lett.*, **43**, pp. 452-454 (2007).

[24] A. T. Alastalo, T. Mattila and H. Seppä, "Analysis of a MEMS transmission line", *IEEE Trans. Microwave Theory and Tech.*, **51**, pp. 1977-1981 (2003).

[25] A. T. Alastalo, J. Kiihamäki and H. Seppä, "Microelectromechanical delay lines with slow signal propagation", *J. Micromech. Microeng.*, **16**, pp. 1854-1860 (2006).

[26] L. D. Landau and E. M. Lifshitz, *Mechanics*, Butterworth-Heinemann (1999).

[27] V. Kaajakari, T.Mattila, A. Oja and H. Seppä, "Non-linear limits for single-crystal silicon microresonators", *J. Microelectromech. Syst.*, **13**, pp. 715-724 (2004).

[28] D. Salt, *Handbook of quartz crystal devices*, Wan Nostrand Raynhold (1987).

[29] S.-H. Tseng, Y.-J. Hung, Y.-Z. Juang and M. S.-C. Lu, "A 5.8-GHz VCO with CMOS-compatible MEMS inductors", *Sensors and Actuators A: Physical*, **139**, pp. 187-193 (2007).

[30] N. Yoshizawa, I. Yamamoto and Y. Shimada, “Magnetic field sensing by an electrostrictive/magnetostrictive composite resonator”, *IEEE Trans. Magnetics*, **41**, pp. 4359-4361 (2005).
[31] D. Lange, C. Hagleitner, C. Herzog, O. Brand and H. Baltes, “Magnetic actuation and MOS-transistor sensing for CMOS-integrated resonators”, *15th IEEE Conference on Micro Electro Mechanical Systems 2002 (IEEE MEMS 2002)*, pp. 304-307 (2002).
[32] B. P. Otis and J. M. Rabaey, ” A 300μW 1.9-GHz CMOS oscillator utilizing micromachined resonators”, *IEEE Journal of Solid-state Circuits*, **38**, pp. 1271-1274 (2003).
[33] D.B. Leeson, “A simple model of feedback oscillator noise spectrum”, *Proc. IEEE*, **54**, pp. 329-330 (1966).
[34] T. Lee, *The design of CMOS radio-frequency integrated circuits*, Cambridge University Press (1998).
[35] V. Kaajakari, J. K. Koskinen and T. Mattila ”Phase-noise in capacitively coupled micromechanical oscillators”, *IEEE Trans. Ultrason., Ferroelect., Freq. Contr.*, **52**, pp. 2322-2331 (2005).
[36] V. Kaajakari, T. Mattila, J. Kiihamäki, H. Kattelus, A. Oja and H. Seppä, ”Square-extensional Mode Single-Crystal Silicon Micromechanical Resonator”, in *12th International Conference on Solid-State Sensors, Actuators and Microsystems (Transducers ’03)*, pp. 951-954 (2003).
[37] V. Kaajakari, T. Mattila, A. Oja, J. Kiihamäki, and H. Seppä, ”Square-extensional mode single-crystal silicon micromechanical resonator for low phase noise oscillator applications”, *IEEE Electron Device. Lett.* **25**, pp. 173-175 (2004).
[38] S. Lee, M. U. Demirci and C. T.-C. Nguyen, “A 10 MHz Micromechanical Resonator Pierce Reference Oscillator for Communications”, in *11th International Conference on Solid-state sensors and actuators (Transducers ’01)*, pp. 1094-1097 (2001).
[39] T. Mattila, O. Jaakkola, J. Kiihamäki, J. Karttunen, T. Lamminmäki, P. Rantakari, A. Oja, H. Seppä, H. Kattelus and I. Tittonen, ”14 MHz micromechanical oscillator”, *Sensors and Actuators A: Physical*, **97-98**, pp. 497-502 (2002).
[40] T. Mattila, J. Kiihamäki, T. Lamminmäki, O. Jaakkola, P. Rantakari, A. Oja, H. Seppä, H. Kattelus and I. Tittonen, ”12 MHz micromechanical bulk acoustic mode oscillator”, Sensors and Actuators A: Physical, **101**, pp. 1-9 (2002).
[41] P. Rantakari, V. Kaajakari, T. Mattila, J. Kiihamaki, A. Oja, I. Tittonen and H. Seppä, “Low noise, low power micromechanical oscillator” in *13th International Conference on Solid-State Sensors, Actuators and Microsystems, (Transducers’05)*, pp. 2135-2138 (2005).
[42] L. Yu-Wei, L. Seungbae, L. Sheng-Shian, X. Yuan, R. Zeying and C.T.-C. Nguyen, “Series-Resonant VHF Micromechanical resonator reference oscillators”, *IEEE Journal of Solid-State Circuits*, **39**, pp. 2477-2491 (2004).
[43] Yu-Wei, L. Sheng-Shian, R. Zeying and C.T.-C. Nguyen, “Low Phase Noise Array-Composite Micromechanical Wine-Glass Disk Oscillator”, in *IEEE Electron Devices Meeting 2005 (IEDM 2005)*, pp. 287-290 (2005).
[44] V. Kaajakari, P. Rantakari, J. K. Koskinen, T. Mattila, J. Kiihamäki, M Koskenvuori, I. Tittonen and A. Oja, ”Low noise silicon micromechanical bulk acoustic wave oscillator”, in *IEEE Ultrasonics Symposium 2005*, pp. 1299-1302 (2005).
[45] IEEE 802.15.4: *IEEE Standard for Information technology- Telecommunications and information exchange between systems- Local and metropolitan area networks- Specific requirements Part 15.4: Wireless Medium Access Control (MAC) and Physical Layer (PHY) Specifications for Low-Rate Wireless Personal Area Networks (WPANs).*
[46] IEEE 802.15.3: *IEEE standard for information technology - telecommunications and information exchange between systems - local and metropolitan area networks - specific requirements part 15.3: wireless medium access control (MAC) and physical layer (PHY) specifications for high rate wireless personal area networks (WPANs).*
[47] IEEE 802.15.1: *IEEE Std 802.15.1 - 2005 IEEE Standard for Information technology - Telecommunications and information exchange between systems - Local and metropolitan area networks - Specific requirements. - Part 15.1: Wireless medium access control (MAC) and physical layer (PHY) specifications for wireless personal area networks (WPANs).*
[48] ETSI TS 100 910 V8.20.0: *Digital cellular telecommunications system (Phase 2+); Radio Transmission and Reception (3GPP TS 05.05 version 8.20.0 Release 1999) (1999).*
[49] CCIR Recommendation No. 686: ”Glossary”, CCIR 17th Plenary Assembly, Vol. VII “Standard Frequency and Time Signals (Study Group 7)” (1990).
[50] J. R. Vig and T. R. Meeker, “The aging of bulk acoustic wave resonators, filters and oscillators”, in *45th Annual Symposium on Frequency Control*, pp. 77-101 (1991).
[51] H. Guckel, XXXX, “Polysilicon resonant microbeam technology for high performance sensor applications”, in *5th IEEE Solid- State Sensor and Actuator Workshop*, pp. 153–156 (1992).
[52] C. Bourgeois, E. Steinsland, N. Blanc and N. F. de Rooij, “Design of resonators for the determination of the temperature coefficients of elastic constants of monocrystalline silicon”, *IEEE Int. Freq. Contr. Symp* 1997, pp. 791-799 (1997).

[53] M. Koskenvuori, V. Kaajakari, T. Mattila and I. Tittonen, " Temperature measurement and compensation based on two vibrating modes of a bulk acoustic mode microresonator ", accepted to *21st IEEE International Conference on Micro Electro Mechanical Systems (MEMS'08)* (2008).
[54] R. Melamud, B. Kim, M. A. Hopcroft, S. Chandorkar, M. Agarwal, C. M. Jha and T. W. Kenny, "Composite flexural-mode resonator with controllable turnover temperature", in *IEEE International Conference on Micro Electro Mechanical Systems (MEMS 2007)*, pp. 199-202 (2007).
[55] O. Hahtela, P. Sievilä, N. Chekurov and I. Tittonen, "Atomic layer deposited alumina (Al2O3) thin film on a high-Q mechanical silicon oscillator", *J. Micromech. Microeng.*, **17**, pp. 737-742 (2007).
[56] W.-T. Hsu, J. R. Clark and C. T.-C. Nguyen, "Mechanically temperature-compensated flexural mode micromechanical resonator", in *IEEE International Electron Devices Meeting 2000 (IEDM 2000)*, pp. 399-402 (2000).
[57] T. Mattila, O. Jaakkola, V. Kaajakari, A. Oja and H. Seppä, "Frequency synthesizer", US Patent US2005285692, (2005).
[58] R. Kazinczi, *Reliability of micromechanical thin-film resonators*, PhD Thesis, TU-Delft (2002).
[59] J. R. Barnes, R. J. Stephenson, C. N. Woodburn, S. J. O'Shea, and M. E. Welland, T. Rayment, J. K. Gimzewski and Ch. Gerber, "A femtojoule calorimeter using micromechanical sensors", *Rev. Sci. Instrum.*, **65**, pp. 3793-3798 (1994).
[60] R. T. Howe and R. S. Muller, "Resonant-microbridge vapor sensor", *IEEE Trans. Electron Devices*, **33**, pp. 499 - 506 (1986).
[61] T. Ono, D. F. Wang, and M. Esashi, "Mass sensing with resonating ultrathin double beams", in *IEEE Sensors 2003*, pp. 825 - 829 (2003).
[62] W. W. van Arsdell and S. B. Brown, "Subcritical Crack Growth in Silicon MEMS", *J. Microelectromech. Syst,* **8** pp. 319-327 (1999).
[63] M. Koskenvuori, T. Mattila, A. Häärä, J. Kiihamäki, P. Rantakari, A. Oja, H. Seppä and I. Tittonen, "Major improvement of long-term stability of SOI-microresonators by encapsulation", in *Eurosensors XVIII*, pp. 550-551 (2004).
[64] V. Kaajakari, J. Kiihamäki, A. Oja, S. Pietikäinen, V. Kokkala and H. Kuisma, "Stability of wafer level vacuum encapsulated single-crystal silicon resonators", *Sensors and Actuators A: Physical*, **130-131**, pp. 42-47 (2006).
[65] B. Kim, R. N. Candler, M. A. Hopcroft, M. Agarwal, W.-T. Park and T. W. Kenny, "Frequency stability of wafer-scale film encapsulated silicon based MEMS resonators", *Sensors and Actuators A: Physical*, **136**, pp. 125-131 (2007).
[66] J. A. Henry, Y. Wang and M. A. Hines, "Controlling energy dissipation and stability of micromechanical silicon resonators with self-assembled monolayers", *Appl. Phys. Lett.,* **84**, pp. 1765-1767 (2004).
[67] A. Kärkkäinen, N. Tisnek, A. Manninen, N. Pesonen, A. Oja and H. Seppä, "Electrical stability of a MEMS-based AC voltage reference", *Sensors and Actuators A: Physical*, **137**, pp. 169-174 (2007).
[68] A. Kärkkäinen, *MEMS based voltage references*, Doctoral Thesis, Helsinki University of Technology (VTT Publications, Espoo) (2006).
[69] A. Kärkkäinen, S.A. Awan, J. Kyynäräinen, P. Pekko, A. Oja and H. Seppä, "Optimized design and process for making a voltage reference based on MEMS", *IEEE Trans. Instrumentation and measurement*, **54**, pp. 563-566 (2005).
[70] R. W, Herfst, H. G. A. Huizing, P. G. Steeneken, and J. Schmitz, "Characterization of dielectric charging in RF MEMS capacitive switches", *IEEE International Conference on Microelectronic Test Structures*, pp. 133-136 (2006).
[71] V. Kaajakari, A. T. Alastalo and T. Mattila, "Electrostatic transducers for micromechanical resonators: Free space and solid dielectric", *IEEE Trans. Ultrason., Ferroelect., and Freq. Contr.,* **53**, pp. 2484-2489 (2006).
[72] I. Kuehne, A. Frey, D. Marinkovic, G. Eckstein and H. Seidel, „Power MEMS – A capacitive vibration-to-electrical energy converter with buil-in voltage", *Sensors and Actuators A: Physical* (Article in press) (2007).
[73] N. W. Ashcroft and N. D. Mermin, *Solid State Physics* (Philadelphia: Holt, Rinehart and Winston) (1976).
[74] S. M. Sze, *Semiconductor devices 2nd ed*., John Wiley & Sons Ltd (2002).
[75] W. Mönch, *Semiconductor Surfaces and Interfaces*, Springer (1995).
[76] T. Durakiewicz, A. Arko, J. J. Joyce, D. P. Moore and S. Halas "Thermal work function shifts for polycrystalline metal surfaces" *Surf. Sci,*. **478** pp. 72-82 (2001).
[77] H. Lüth H, *Surfaces and Interfaces of Solid Materials*, Springer (1998).
[78] J. Pohjanen, *Sähköstaattiset pintailmiöt kapasitiivisessa kyhtyvyysanturissa*, M. Sc. Thesis, Tampere University of Technology (2003).
[79] V.-P. Rytkönen, *Built-in voltages of metal semiconductor junctions and structures*, M. Sc. Thesis, Helsinki University of Technology (2005).
[80] C. L. Goldsmith, J. Ehmke, A. Malczewski, B. Pillans, S. Eshelman, Z. Yao, J. Brank and M. Eberly, "Lifetime characterization of capacitive RF MEMS switches" *Tech. Dig. IEEE MTT-S Int. Microwave Symp.* 2001, pp. 227-230 (2001).

[81] W. Merlijin van Sprengen, R. Puers, R. Mertens and I de Wolf, "A comprehensive model to predict the charging and reliability of capacitive RF MEMS switches", *J. Micromech. Microeng.*, **14**, pp. 514-521 (2004).
[82] B. Bircumshaw, G. Liu, H. Takeuchi, K. Tsu-Jae, R. Howe, O. O'Reilly and A. Pisano, "The radial bulk annular resonator: towards a 50 Ω RF MEMS filter", in *12th International Conference on Solid-State Sensors, Actuators and Microsystems (Transducers '03),* pp. 875-878 (2003).
[83] X. Yuan, L. Sheng-Shian, L. Yu-Wei, R. Zeying and C. -T. C. Nguyen., "UHF micromechanical extensional wine-glass mode ring resonator", in IEEE International Electron Devices Meeting 2003 (*IEDM 2003)*, pp. 39.2.1-39.2.4 (2003).
[84] J. Wang, Z. Ren and C. T.-C. Nguyen, "1.156-GHz self-aligned vibrating micromechanical disk resonator", *IEEE Trans. Ultrason., Ferroelect., Freq. Contr.*, **51**, pp. 1607-1628 (2004).
[85] R. B. Reichenbach, M. Zalalutdinov, K. L. Aubin, R. Rand, B. H. Houston, J. M. Parpia and H. G. Craighead, "Third-order intermodulation in a micromechanical thermal mixer", *J. Micromech. Microeng.*, **14**, pp. 1244-1252 (2005).
[86] B. Razavi, *RF Microelectronics*, Prentice Hall PTR (1998).
[87] R. Navid, J. R. Clark, M. demirci and C. T.C. Nguyen, "Third-order intermodulation distortion in capacitively-driven CC-beam micromechanical resonators", in *14th IEEE International Conference Micro Electro Mechanical Systems 2001 (MEMS 2001)*, pp. 228-231 (2001).
[88] A. T. Alastalo and V. Kaajakari, "Intermodulation in Capacitively Coupled Microelectromechanical Filters", *IEEE Electron Device Lett.*, **26**, pp. 289-291 (2005).
[89] T. Mattila and T. Veijola, "Modelling of non-linear micromechanical resonators and their simulation with the harmonic-balance method", *Int. J. RF. Microw. CAE*, **11**, pp. 310-321 (2001).
[90] S. Maas, *Non-linear microwave and RF-circuits*, Artech house (2003).
[91] J.L. Lopez, J. Teva, A. Uranga, F. Torres, J. Verd, G. Abadal and N. Barniol, "Mixing in a 220 MHz CMOS-MEMS", in *IEEE International symposium on Circuits and Systems 2007 (ISCAS 2007)*, pp. 2630–2633 (2007).
[92] S-S. Li, Y-W. Lin, Y. Xie, Z. Ren and C. T.C. Clark, "Small percentage bandwidth design of a 423-MHz notch-coupled micromechanical mixler", in *IEEE Ultrasonics Symposium 2005*, pp. 1295-1298 (2005).
[93] D. Rugar and P Gutter, "Mechanical parametric amplification and thermomechanical noise squeezing", *Phys. Rev. Lett.*, **67**, pp. 699-702 (1991).
[94] D. W. Carr, S. Evoy, L. Sekaric, H. G. Craighead, and J. M. Parpia, "Parametric amplification in a torsional microresonator", *Appl. Phys. Lett.*, **77**, pp. 1545-1547 (2000).
[95] M. Zalalutdinov, A. Olkhovets, A. Zehnder, B. Ilic, D. Czaplewski, H. G. Graighead and J. M. Parpia, "Optically pumped parametric amplification for micromechanical oscillators", *Appl. Phys. Lett.*, **78**, pp. 3142-3144 (2001).
[96] B. E. DeMartini, J. F. Rhoades, K. L. Turner, S. W. Shaw and J. Moehlis, "Linear and nonlinear tuning of parametrically excited MEMS oscillators", *J. Microelectromech. Syst.*, **16**, pp. 310-318 (2007).
[97] W. Zhang, R. Baskaran and K. L. Turner, "Effect of cubic nonlinearity on auto-parametrically amplified resonant MEMS mass sensor", *Sensors and Actuators A: Physical*, **102**, pp. 139-150 (2002).
[98] W. M. Dougherty, K. J. Brauland, J. L. Garbini and J. A. Sidles, "Detection of AC magnetic signals by parametric mode coupling in a mechanical oscillator", *Meas. Sci. Technol.*, **7**, pp. 1733-1739 (1996).
[99] T. Ono, H. Wakamatsu and M. Esashi, "Parametrically amplified thermal resonant sensor with pseudo-cooling effect", *J. Micromech. Microeng.*, **15**, pp. 2282-2288 (2005).
[100] J. F. Rhoades, S. W. Shaw, K. L. Turner and R. Baskaran, "Tunable microelectromechanical filters that exploit parametric resonance", *J. Vibration Acoust.*, **127**, pp. 423-430 (2005).
[101] Aplac RF Design Tool, AWR-Aplac Corp. [Online] Available: www.aplac.com.
[102] J. C. Arnold and H. H. Sawin, "Charging of pattern features during plasma etching", *J. Appl. Phys.*, **70**, pp. 5314-5317 (1991).
[103] C. Iliescu and J. Miao, "One-mask process for silicon accelerometers on Pyrex glass utilising notching effect in inductively coupled plasma DRIE", *Electron. Lett.* **39**, pp.658-659 (2003).
[104] L. Haobing and F. Chollet, J., "Layout controlled one-step dry etch and release of MEMS using deep RIE on SOI wafer", *J. Microelectromech. Syst.,* **15**, pp.541-547 (2006).
[105] P. T. Docker, P. Kinnell and M. C. L. Ward, J., "A dry single-step process for the manufacture of released MEMS structures", *J. Micromech. Microeng.*, **13**, pp. 790-794 (2003).
[106] W Zhang, W Zhang, K. Turner and P. G. Hartwell, "Scream'03: A single mask process for high-Q single crystal silicon MEMS", in ASME International Mechanical Engineering Congress and Exposition 2004 (IMECE04), paper nr. 61140 (2004).
[107] R. B. Bosch GbmH *US Patent* 4855017, *Germany Patent* 4241045CI (1994).
[108] K. Grigoras, L. Sainiemi, J. Tiilikainen, A. Säynätjoki, V-M. Airaksinen and S. Franssila, "Application of ultra-thin aluminium oxide etch mask made by atomic layer deposition technique", *J. Phys. Conf . Series* **61** pp. 369-374 (2007).
[109] C. K. Chung, "Geometrical pattern effect on silicon deep etching by an inductively coupled plasma system", *J. Micromech. Microeng*., **14**, pp. 656-662 (2003).

[110] M. Koskenvuori and I. Tittonen, ”Towards micromechanical radio: GHz-range communication with micromechanical resonators”, *Eurosensors XX*, pp. 332-333 (2006).
[111] M. Koskenvuori, P. Rantakari, T. Lamminmäki, I. Tittonen, A. Oja, T. Mattila, H. Seppä, J. Kiihamäki and H. Kattelus, ”Enhancing the electromechanical coupling in bulk acoustic mode microresonator”, *Eurosensors XVI*, pp.383-384 (2002)
[112] A. Oja, T. Mattila, H. Seppä, J. Kiihamäki, H. Kattelus, T. Lamminmäki, M. Koskenvuori, P. Rantakari and I. Tittonen, ”Nonlinear effects in bulk acoustic mode microresonators”, *Eurosensors XVI*, pp. 381-382 (2002)

Appendix I – Derivation of the force for AM-modulated signal

If the input signal is

$$U(t) = [A_0 + B_0 \cos(2\omega_m t)]\cos(\omega_c t)$$
$$= A_0\left[\cos(\omega_c t) + \frac{h}{2}\cos(\omega_c \pm \omega_m)t\right] ,$$

where modulation index h is defined $h = B_0/A_0$

And this is applied to capacitive transducer with the force-voltage relationship as (1.6) the components of force arising are

$$F = \frac{A_0^2}{4}\frac{\partial C}{\partial x}\left\{1 + \frac{h^2}{2} - \cos(2\omega_c t) + \right.$$
$$- \frac{h^2}{4}[\cos 2(\omega_c \pm \omega_m)t]$$
$$+ \frac{h^2}{4}(\cos 2\omega_m t + \cos 2\omega_c t) + \qquad \text{(A-1.1)}$$
$$- h\cos(2\omega_c \pm \omega_m)t \; +$$
$$\left. + 2h\cos\omega_m t \right\},$$

where the last term represents the components of force at the frequency $f_m = f_0$.

$$F\big|_{\omega_m} = \frac{1}{2}A_0^2 h\frac{\partial C}{\partial x} = \frac{1}{2}A_0 B_0\frac{\partial C}{\partial x}.$$

ISBN 978-951-22-9278-3
ISBN 978-951-22-9279-0 (PDF)
ISSN 1795-2239
ISSN 1795-4584 (PDF)